Received 11 August 2008
Revised 11 November 2008
and 2 December 2008
Accepted 15 December 2008

Impulsive Falkner-Skan flow with constant wall heat flux: revisited

Simon D. Harris
Rock Deformation Research, School of Earth Sciences, University of Leeds, Leeds, UK
Derek B. Ingham
Centre for Computational Fluid Dynamics, Faculty of Engineering, School of Process, Environmental and Materials Engineering, University of Leeds, Leeds, UK, and
Ioan Pop
Faculty of Mathematics, University of Cluj, Cluj, Romania

Abstract

Purpose – The purpose of this paper is to present a numerical and an analytical study of the fluid flow and heat transfer in the unsteady, laminar boundary layer resulting from the forced convection flow along a semi-infinite wedge, where the transients are initiated at time $\bar{t} = 0$ when the wedge is impulsively started from rest with a uniform velocity and a constant heat flux at the walls of the wedge is suddenly imposed.

Design/methodology/approach – The velocity of the main free stream is written in non-dimensional form for $t > 0$ as $u_e(x) = x^m$, where x is the non-dimensional distance along the surface from the leading edge (apex) of the wedge and the constant m is related to the included angle of the wedge $\pi\beta$ by $m = \beta/(2-\beta)(0 \leq m \leq 1$ for physical applications). The wedge and the fluid are assumed to be initially ($\bar{t} = 0$) at the same uniform temperature T_∞, so that there is zero heat flux at the surface. A time-dependent thermal boundary layer is then produced at $\bar{t} = 0$ as the zero heat flux at the surface is suddenly changed, and a constant heat flux q_w is imposed as the wedge is set into motion. Analytical solutions for the simultaneous development of the momentum and thermal boundary layers are obtained for both small (initial unsteady flow) and large (steady-state flow) times for several wedge angles (several values of m) and several values of the Prandtl number Pr. These two asymptotic solutions are matched using two specialised numerical procedures.

Findings – The numerical results obtained for the transient fluid velocity and temperature fields concentrate mainly on the case when the Prandtl number $\mathrm{Pr} = 1$ and $m = 1/5$, namely a wedge angle of 60°. Required alterations to these parameters are then discussed with reference to variations in Pr and m separately. Further, an engineering empirical expression is presented for the skin friction $C_f(\tau)\mathrm{Re}_x^{1/2}$ that is valid for all times. The comparison between the empirical formula and the full numerical solution demonstrates that this matching solution can be used with confidence over the whole range of values of the non-dimensional time τ for each of the values of m presented, and may therefore be used with confidence in engineering applications.

Originality/value – The results of the present work, which have been obtained through many computations, are very important for the advancement of knowledge on this classical problem of fluid mechanics and heat transfer. It is believed that such very detailed solutions have not previously been presented.

Keywords Flow, Heat, Flux, Boundary layers
Paper type Research paper

International Journal of Numerical Methods for Heat & Fluid Flow
Vol. 19 No. 8, 2009
pp. 1008-1037

0961-5539
DOI 10.1108/09615530910994478

The authors wish to express their very sincere thanks to the reviewers for their valuable comments and suggestions. Also, two of the authors, D. B. Ingham and I. Pop, gratefully acknowledge some financial support from The Royal Society.

1. Introduction

The unsteady nature of a wide range of fluid flows of practical importance has received considerable attention in recent years. In many applications, the ideal flow environment around the device is nominally steady, but undesirable unsteady effects arise either due to self-induced motions of the body, or due to fluctuations or non-uniformities in the surrounding fluid. Unsteady viscous flows have been studied rather extensively and all of the characteristic features of unsteady effects are now more or less familiar to fluid mechanists. Comprehensive reviews of the literature on unsteady forced convection boundary-layer flows are presented in Riley (1975, 1990), Telionis (1979, 1981), and Ludlow *et al.* (2000). However, fewer studies have been concerned with the forced convection heat transfer aspects, see Pop (1996).

The boundary-layer flow along a semi-infinite flat plate that is started impulsively from rest was first studied by Stewartson (1951), Hall (1969), Dennis (1972), and others. Extending the work of Stewartson (1951), Smith (1967) considered the impulsive motion of a wedge and presented an approximate solution that is based on the momentum integral method. Nanbu (1971) obtained numerical solutions of this problem, using a scheme similar to that of Hall (1969), i.e. using three independent variables. Williams and Rhyne (1980) formulated the problem of impulsively set into motion wedge type (Falkner-Skan) flows in a new set of scaled coordinates. Both the short-time solution and the solution for infinite time, the Falkner-Skan solution, were included in this new formulation of the problem. In addition, the new scaling reduced the region of integration from the traditional infinite region to a finite region, thus also reducing the time required for numerical computations. Numerical solutions for the forced convection thermal boundary layer produced by the sudden imposition of a constant temperature difference between the wedge and the fluid as the motion is started have been given by Watkins Jr (1976). Very recently, Xu and Pop (2008) have studied the unsteady boundary-layer flow past a wedge using the homotopy analytic method (HAM). The problem of a wedge impulsively set into motion and some associated heat transfer characteristics have been considered by Harris *et al.* (2002, 2008).

The purpose of this work is to study the forced convection heat transfer in the unsteady, thermal boundary layer associated with the forced convection (momentum) boundary-layer flow resulting from a transient Falkner-Skan problem with exponent m initiated by a sudden change in the thermal boundary condition to a uniform wall heat flux. This situation has physical relevance when $0 \leq m \leq 1$, and for such cases the flow is that of an incompressible fluid past a sharp, semi-infinite wedge of included angle $2m\pi/(m+1)$. The surface is set impulsively into motion at (non-dimensional) time $t = 0$ with a (non-dimensional) potential flow $u_e(x) = x^m$. Both the fluid and the surface are initially at a constant temperature and the transients are initiated when the zero heat flux at the surface is suddenly changed to a constant value. The initial (unsteady) development of the thermal boundary layer is satisfactorily represented by a series solution for small times. Physically, at this stage, diffusion dominates convection, which is affected only weakly by the velocity components close to the wedge. The solution for large times (steady state) is given by the Falkner-Skan equation. For small times the flow is generally independent of the conditions far upstream, but at the leading edge and for large times the flow depends on these solutions. The mathematical problem for small times is governed by the Rayleigh type of equation and for large times by the Falkner-Skan type of equation. The results obtained for the heat transfer characteristics during the initial and final stages of the motion are supplemented by a numerical integration of the transformed

boundary-layer equations. The detailed numerical solution presented here for the whole transient from the initial ($t = 0$) unsteady to the final ($t \to \infty$) steady state consists of a modification of the step-by-step method proposed by Merkin (1972) in combination with a finite-difference method similar to that proposed by Dennis (1972), which has been very successfully used recently on a range of problems by Harris *et al.* (1997a, b, 1998, 1999, 2001, 2002, 2008). Particular cases of the present results are compared with those of Hartree (1937). It may be noted that here the heat transfer problem is not the same as in other works (Watkins, Jr, 1976; Tsay and Shih, 1979; Bhattacharyya and Gupta, 1996; Harris *et al.* 2002), where the thermal boundary layer is due to a sudden change in the surface temperature of the wedge. Some recent work on steady or unsteady boundary-layer flow and heat transfer past a wedge has, however, been performed by Cheng and Lin (2002), Kuo (2003), and Pantokratoras (2006). It should be mentioned that the present results, which have been obtained through many computations, are very important for the advancement of our knowledge on this classical problem of fluid mechanics and heat transfer. To our knowledge such very detailed solutions have not previously been presented.

2. Basic equations

The generalized impulsive Falkner-Skan system that we consider is based upon the problem of the unsteady, two-dimensional, viscous flow of an incompressible fluid past a symmetrical, sharp wedge with an $\bar{x}$ and $\bar{y}$ coordinate system, where $\bar{x}$ is measured along the surface of the wedge from the apex and $\bar{y}$ is measured normal to the surface; see Figure 1. At time $\bar{t} = 0$, the wedge is impulsively set into motion with a uniform speed U_∞ along its plane of symmetry in an otherwise stationary, viscous, and incompressible fluid. The heat transfer problem is idealised as follows. The wedge and the fluid are assumed to be initially at the same uniform temperature T_∞, so that there is zero heat flux at the surface. A time-dependent thermal boundary layer is then produced at $\bar{t} = 0$ as the zero heat flux at the surface is suddenly changed, and a constant heat flux q_w is imposed as the wedge is set into motion. The inviscid flow over the wedge develops instantaneously and its velocity is given by:

$$\bar{u}_e(\bar{x}) = U_\infty \left(\frac{\bar{x}}{l}\right)^m, \tag{1}$$

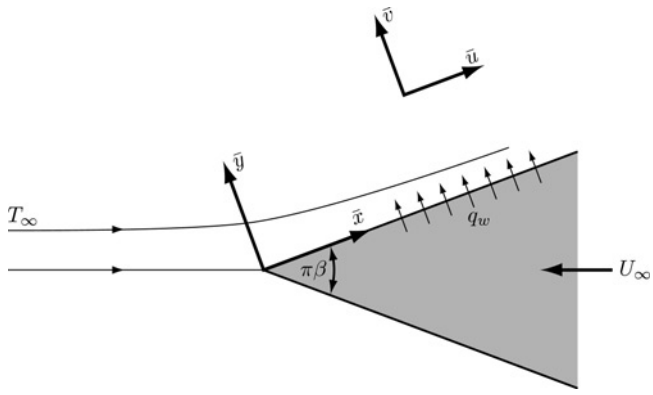

Figure 1.
Physical model and coordinate system

where l is a characteristic length and m is related to the included angle $\pi\beta$ by $m = \beta/(2-\beta)$. It is clear that for negative values of m the solution becomes singular at $\bar{x} = 0$, whilst for m positive the solution can be defined for all values of $\bar{x}$, and this leads to a general difference between the solutions for the cases of $m < 0$ and $m \geq 0$. The particular cases of Blasius' solution for a flat plate ($\beta = 0$, $m = 0$), stagnation point flow ($\beta = 1$, $m = 1$), together with the wedge angles 30° ($\beta = 1/6, m = 1/11$), 60° ($\beta = 1/3, m = 1/5$), and 90° ($\beta = 1/2, m = 1/3$), will be considered for several values of the Prandtl number, Pr. We will also consider in more detail the steady flow case ($\tau \to \infty$), described by the Falkner-Skan equation, for one further value of the parameter m, namely $m = 2(\beta = 4/3)$, corresponding to a wedge angle of 240°. For physical applications we require that $0 \leq \beta \leq 1$ ($0 \leq m \leq 1$), since the acute wedge angle is $\pi\beta$, and this upper limit corresponds to $m = 1$. Other values of m will be considered within the Blasius-like solution range $m^* \leq m < \infty$, where m^* is the minimum value of m for which boundary-layer separation occurs. When $m^* \leq m < 0$ and $m > 1$, the situation is no longer physically relevant with respect to the acute, semi-infinite wedge problem. However, such cases are of considerable mathematical interest and have intrigued the applied mathematics community for many years.

We introduce non-dimensional variables according to:

$$\begin{aligned} x &= \frac{\bar{x}}{l}, \quad y = \mathrm{Re}^{1/2}\frac{\bar{y}}{l}, \quad u = \frac{\bar{u}}{U_\infty}, \quad v = \mathrm{Re}^{1/2}\frac{\bar{v}}{U_\infty}, \\ u_e &= \frac{\bar{u}_e}{U_\infty}, \quad t = \frac{U_\infty}{l}\bar{t}, \quad T = \frac{k_f}{l q_w}\mathrm{Re}^{1/2}(\bar{T} - T_\infty), \end{aligned} \tag{2}$$

where $\mathrm{Re} = U_\infty l/\nu$ is the Reynolds number, $\bar{u}$ and $\bar{v}$ are the velocity components along the $\bar{x}$- and $\bar{y}$- axes, respectively, $\bar{T}(\bar{x}, \bar{y}, \bar{t})$ is the fluid temperature, ν is the kinematic viscosity, and k_f is the thermal conductivity of the fluid. The velocity over the wedge, see Equation (1), is now given by:

$$u_e(x) = x^m \tag{3}$$

and, sufficiently far downstream from the apex, the governing equations in the boundary layer can be written in non-dimensional form as (see Harris *et al.*, 2002, 2008):

$$\frac{\partial u}{\partial x} + \frac{\partial v}{\partial y} = 0, \tag{4}$$

$$\frac{\partial u}{\partial t} + u\frac{\partial u}{\partial x} + v\frac{\partial u}{\partial y} = u_e\frac{\mathrm{d}u_e}{\mathrm{d}x} + \frac{\partial^2 u}{\partial y^2}, \tag{5}$$

$$\frac{\partial T}{\partial t} + u\frac{\partial T}{\partial x} + v\frac{\partial T}{\partial y} = \frac{1}{\mathrm{Pr}}\frac{\partial^2 T}{\partial y^2}, \tag{6}$$

under the assumption of the boundary-layer approximation and negligible viscous dissipation. Equations (4)-(6) must be solved subject to the following initial and boundary conditions:

$$\left.\begin{array}{ll} u=0, \quad v=0, \quad T=0 & \text{for all } x, y \quad \text{for } t<0, \\ u=0, \quad v=0, \quad \dfrac{\partial T}{\partial y}=-1 & \text{on } y=0, \ x>0 \\ u \to u_e(x), \quad T \to 0 & \text{as } y \to \infty, \ x>0 \end{array}\right\} \quad \text{for } t \geq 0 \tag{7}$$

The number of independent variables in the governing equations can be reduced from three to two by introducing the non-dimensional, reduced stream function $f(\eta, \tau)$ and the non-dimensional, reduced temperature function $g(\eta, \tau)$ according to:

$$\psi = x^{(m+1)/2} f(\eta, \tau), \qquad T = x^{(1-m)/2} g(\eta, \tau), \quad \eta = x^{(m-1)/2} y, \quad \tau = x^{m-1} t, \tag{8}$$

where η is a non-dimensional similarity variable and ψ is the stream function, which is defined in the usual way, namely $u = \partial\psi/\partial y$ and $v = -\partial\psi/\partial x$. Substituting the transformation (8) into Equations (5) and (6), we obtain:

$$\begin{aligned} \frac{\partial^3 f}{\partial \eta^3} + \left[\frac{m+1}{2} f + (m-1)\tau \frac{\partial f}{\partial \tau}\right] \frac{\partial^2 f}{\partial \eta^2} + m\left[1 - \left(\frac{\partial f}{\partial \eta}\right)^2\right] \\ = \left[1 + (m-1)\tau \frac{\partial f}{\partial \eta}\right] \frac{\partial^2 f}{\partial \eta \partial \tau}, \end{aligned} \tag{9}$$

$$\begin{aligned} \frac{1}{\mathrm{Pr}} \frac{\partial^2 g}{\partial \eta^2} + \left[\frac{m+1}{2} f + (m-1)\tau \frac{\partial f}{\partial \tau}\right] \frac{\partial g}{\partial \eta} - \frac{1-m}{2} g \frac{\partial f}{\partial \eta} \\ = \left[1 + (m-1)\tau \frac{\partial f}{\partial \eta}\right] \frac{\partial g}{\partial \tau}, \end{aligned} \tag{10}$$

respectively, and the boundary conditions (7) become:

$$\begin{aligned} f(0,\tau) = 0, \quad \frac{\partial f}{\partial \eta}(0,\tau) = 0, \quad \frac{\partial g}{\partial \eta}(0,\tau) = -1, \\ \frac{\partial f}{\partial \eta}(\eta,\tau) \to 1, \quad g(\eta,\tau) \to 0 \quad \text{as } \eta \to \infty, \end{aligned} \tag{11}$$

for $\tau \geq 0$.

The quantities of physical interest in this problem are the skin friction coefficient C_f and the non-dimensional wall temperature $T_w(x, t)$, which are defined as:

$$C_f = \frac{\tau_w(\bar{x})}{\rho(\bar{u}_e(\bar{x}))^2}, \quad T_w(x,t) = T(x,0,t) = \frac{k_f}{l q_w} \mathrm{Re}^{1/2} (\bar{T}_w(\bar{x}, \bar{t}) - T_\infty), \tag{12}$$

where $\tau_w(\bar{x}) = \mu(\partial \bar{u}/\partial \bar{y})|_{\bar{y}=0}$ is the skin friction along the surface, ρ is the fluid density, and μ is the coefficient of viscosity. By introducing the non-dimensional variables (2) and the transformation (8), we obtain:

$$C_f = \mathrm{Re}_x^{-1/2} \frac{\partial^2 f}{\partial \eta^2}(0,\tau), \quad T_w(x,t) = x^{(1-m)/2} g_w(\tau), \tag{13}$$

where $g_w(\tau) = g(0, \tau)$ and $\mathrm{Re}_x = \bar{u}_e(\bar{x})\bar{x}/\nu$ is the local Reynolds number. We shall refer to $\partial^2 f/\partial\eta^2(0, \tau)$ and $g_w(\tau)$ as the non-dimensional, reduced skin friction coefficient and surface temperature, respectively.

Attention may now be directed toward finding solutions of Equations (9)-(11). Due to the difference in the boundary-layer characteristics between the small-time and large-time solutions, two approximate asymptotic solutions will be sought in these two time regimes.

3. Small-time solution, $\tau \ll 1$

Equations (9) and (10) must now be written in a form that is more convenient for analysis at small times. In all impulsive changes in temperature or heat flux problems there is a short period during which the effects are confined to a thin, one-dimensional boundary layer that is adjacent to the surface. Since the appropriate length scale for small times is the diffusion scale $\tau^{1/2}$, we introduce the following variables:

$$f = 2\tau^{1/2}F(\zeta, \tau), \quad g = 2\tau^{1/2}G(\zeta, \tau), \quad \zeta = \frac{\eta}{2\tau^{1/2}}. \tag{14}$$

Substituting these variables into Equations (9) and (10) yields:

$$\frac{\partial^3 F}{\partial\zeta^3} + \left[2\zeta + 4m\tau F + 4(m-1)\tau^2\frac{\partial F}{\partial\tau}\right]\frac{\partial^2 F}{\partial\zeta^2} + 4m\tau\left[1 - \left(\frac{\partial F}{\partial\zeta}\right)^2\right] = 4\tau\left[1 + (m-1)\tau\frac{\partial F}{\partial\zeta}\right]\frac{\partial^2 F}{\partial\zeta\partial\tau}, \tag{15}$$

$$\frac{1}{\mathrm{Pr}}\frac{\partial^2 G}{\partial\zeta^2} + \left[2\zeta + 4m\tau F + 4(m-1)\tau^2\frac{\partial F}{\partial\tau}\right]\frac{\partial G}{\partial\zeta} - 2G = 4\tau\left[1 + (m-1)\tau\frac{\partial F}{\partial\zeta}\right]\frac{\partial G}{\partial\tau}, \tag{16}$$

and the corresponding boundary conditions (11) become:

$$F(0, \tau) = 0, \quad \frac{\partial F}{\partial\zeta}(0, \tau) = 0, \quad \frac{\partial G}{\partial\zeta}(0, \tau) = -1, \quad \frac{\partial F}{\partial\zeta}(\zeta, \tau) \to 1, \quad G(\zeta, \tau) \to 0 \quad \text{as } \zeta \to \infty. \tag{17}$$

It can easily be verified that the solutions of Equations (15) and (16) at small values of τ ($\ll 1$) take the following form:

$$F(\zeta, \tau) = F_0(\zeta) + F_1(\zeta)\tau + F_2(\zeta)\tau^2 + \ldots, \quad G(\zeta, \tau) = G_0(\zeta) + G_1(\zeta)\tau + G_2(\zeta)\tau^2 + \ldots. \tag{18}$$

The solutions for F_i and G_i, for $i = 0, 1, 2, \ldots$, are determined by substituting these general forms for $F(\zeta, \tau)$ and $G(\zeta, \tau)$ into Equations (15) and (16) and equating coefficients of powers of τ. The first three resulting systems of ordinary differential equations were solved analytically in Harris *et al.* (2008) and we will not repeat these solutions here. Using these analytical solutions, we can write the small-τ solutions for

the non-dimensional fluid velocity $\partial f/\partial\eta(\eta,\tau)$ function and the non-dimensional fluid temperature $g(\eta,\tau)$ function for $\mathrm{Pr}=1$ as follows:

$$\begin{aligned}\frac{\partial f}{\partial\eta}(\eta,\tau)&=\left.\frac{\partial F(\zeta,\tau)}{\partial\zeta}\right|_{\zeta=\eta/2\tau^{1/2}}=F_0'\left(\frac{\eta}{2\tau^{1/2}}\right)+F_1'\left(\frac{\eta}{2\tau^{1/2}}\right)\tau+F_2'\left(\frac{\eta}{2\tau^{1/2}}\right)\tau^2+\ldots\\&=\operatorname{erf}\left(\frac{\eta}{2\tau^{1/2}}\right)+m\left\{\frac{1}{2}\left(\tau-\frac{\eta^2}{2}\right)\operatorname{erf}\left(\frac{\eta}{2\tau^{1/2}}\right)\operatorname{erfc}\left(\frac{\eta}{2\tau^{1/2}}\right)\right.\\&\quad-\left[\frac{2\tau}{3\pi}+\left(1+\frac{2}{3\pi}\right)\frac{\eta^2}{2}\right]\operatorname{erfc}\left(\frac{\eta}{2\tau^{1/2}}\right)+\frac{1}{2\sqrt{\pi}}\left[1+\frac{4}{3\pi}\right.\\&\quad\left.\left.+3\operatorname{erf}\left(\frac{\eta}{2\tau^{1/2}}\right)\right]\eta\tau^{1/2}\mathrm{e}^{-\eta^2/4\tau}+\frac{2\tau}{\pi}\left(-\frac{2}{3}+\mathrm{e}^{-\eta^2/4\tau}\right)\mathrm{e}^{-\eta^2/4\tau}\right\}\\&\quad+F_2'\left(\frac{\eta}{2\tau^{1/2}}\right)\tau^2+\ldots.\end{aligned}\tag{19}$$

$$\begin{aligned}g(\eta,\tau)&=2\tau^{1/2}G(\zeta,\tau)\big|_{\zeta=\eta/2\tau^{1/2}}=2G_0\left(\frac{\eta}{2\tau^{1/2}}\right)\tau^{1/2}+2G_1\left(\frac{\eta}{2\tau^{1/2}}\right)\tau^{3/2}\\&\quad+2G_2\left(\frac{\eta}{2\tau^{1/2}}\right)\tau^{5/2}+\ldots\\&=-\eta\operatorname{erfc}\left(\frac{\eta}{2\tau^{1/2}}\right)+\frac{2}{\sqrt{\pi}}\tau^{1/2}\mathrm{e}^{-\eta^2/4\tau}\\&\quad+m\left\{\left[\frac{\eta}{2}\left(\tau+\frac{\eta^2}{2}\right)\operatorname{erf}\left(\frac{\eta}{2\tau^{1/2}}\right)+\frac{10}{9\pi}\eta\left(3\tau+\frac{\eta^2}{2}\right)\right.\right.\\&\quad\left.+\frac{4}{3\sqrt{\pi}}\tau^{3/2}\right]\operatorname{erfc}\left(\frac{\eta}{2\tau^{1/2}}\right)+\frac{1}{\sqrt{\pi}}\left[\frac{\eta^2}{2}-\frac{10}{9\pi}(4\tau+\eta^2)\right.\\&\quad\left.\left.-(\tau+\eta^2)\operatorname{erf}\left(\frac{\eta}{2\tau^{1/2}}\right)-\frac{1}{\sqrt{\pi}}\eta\tau^{1/2}\,\mathrm{e}^{-\eta^2/4\tau}\right]\tau^{1/2}\mathrm{e}^{-\eta^2/4\tau}\right\}\\&\quad+2G_2\left(\frac{\eta}{2\tau^{1/2}}\right)\tau^{5/2}+\ldots.\end{aligned}\tag{20}$$

where the primes in Equation (19) denote differentiation with respect to $\zeta=\eta/2\tau^{1/2}$.

The solutions of the ordinary differential systems for the functions $F_2(\zeta)$ and $G_2(\zeta)$ can be achieved using the NAG routine D02HAF. This algorithm solves two-point, boundary-value problems for systems of first-order, ordinary differential equations using a Runge-Kutta-Merson method and a Newton iteration in a shooting and matching technique. In this numerical procedure, the upper range of integration must be specified at some finite value instead of infinity, and we will denote the values of ζ and η corresponding to $\zeta=\infty$ and $\eta=\infty$ by ζ_∞ and η_∞, respectively.

The non-dimensional skin friction coefficient $C_f(\tau)\mathrm{Re}_x^{1/2}=\partial^2 f/\partial\eta^2(0,\tau)$ and the reduced surface temperature g_w can now be expressed as

$$C_f(\tau)\mathrm{Re}_x^{1/2} = \frac{\partial^2 f}{\partial \eta^2}(0,\tau) = \frac{1}{2\tau^{1/2}}\frac{\partial^2 F}{\partial \zeta^2}(0,\tau) = \frac{1}{\sqrt{\pi}}\tau^{-1/2} + \frac{m}{\sqrt{\pi}}\left(1+\frac{4}{3\pi}\right)\tau^{1/2} + \frac{1}{2}F_2''(0)\tau^{3/2} + \ldots,$$

$$g_w(\tau) = g(0,\tau) = 2\tau^{1/2}G(0,\tau) = \frac{2}{\sqrt{\pi \mathrm{Pr}}}\tau^{1/2} + \frac{2}{9}\frac{m}{\pi\sqrt{\pi}}\left\{\frac{1}{\mathrm{Pr}-1}\left[\frac{3}{\sqrt{\mathrm{Pr}}}(1+\mathrm{Pr})^3\tan^{-1}\right.\right. \times \left.\left.\left(\frac{1}{\sqrt{\mathrm{Pr}}}\right) - 6\pi\right] - (11+3\mathrm{Pr})\right\}\tau^{3/2} + 2G_2(0)\tau^{5/2} + \ldots, \quad (21)$$

for $\tau \ll 1$, and in the case of $\mathrm{Pr} = 1$ this solution for the reduced surface temperature takes the following form:

$$g_w(\tau) = \frac{2}{\sqrt{\pi}}\tau^{1/2} + \frac{4}{3}\frac{m}{\sqrt{\pi}}\left(1 - \frac{10}{3\pi}\right)\tau^{3/2} + 2G_2(0)\tau^{5/2} + \ldots, \quad (22)$$

for $\tau \ll 1$.

The results for F_2'' (0) and G_2 (0) were presented in Harris *et al.* (2008) for some values of the parameters m and Pr, based on specifying the upper range of integration at the finite value $\zeta_\infty \approx$ 6-8 (dependent on the values of m and Pr).

4. Large-time solution, $\tau \to \infty$

The transport of energy becomes steady as $\tau \to \infty$ and hence $f(\eta,\tau) = f_\infty(\eta)$ and $g(\eta,\tau) = g_\infty(\eta)$, say, so that Equations (9) and (10) reduce to the following ordinary differential equations:

$$f_\infty''' + \frac{1}{2}(m+1)f_\infty f_\infty'' + m\left(1 - f_\infty'^2\right) = 0, \quad (23)$$

$$\frac{1}{\mathrm{Pr}}g_\infty'' + \frac{1}{2}(m+1)f_\infty g_\infty' - \frac{1}{2}(1-m)f_\infty' g_\infty = 0, \quad (24)$$

which must be solved subject to the boundary conditions:

$$f_\infty(0) = 0, \quad f_\infty'(0) = 0, \quad g_\infty'(0) = -1, \quad f_\infty'(\eta) \to 1, \quad g_\infty(\eta) \to 0 \quad \text{as } \eta \to \infty, \quad (25)$$

where primes now denote differentiation with respect to η.

The stream function $f_\infty(\eta)$ is the well-known Falkner-Skan solution and the properties of this solution, as a function of the parameter m, have been discussed in numerous papers; see, for example, Lin and Lin (1987) and Harris *et al.* (2008). The limiting value $m = m^* = -0.0904285623$ determines the value of m at which the laminar boundary layer breaks away from the surface, so that f_∞'' (0) = 0 at $m = m^*$. The variations in the solutions for the non-dimensional skin friction coefficient f_∞'' (0) and the reduced surface temperature g_∞ (0) in the case of $m \to (m^*)^+$ have been described in Harris *et al.* (2008) for different values of the Prandtl number Pr. Here we

consider solutions for $f''_{\infty}(0)$ and $g_{\infty}(0)$ over the range $m^* \leq m \leq \infty$ and separately consider the cases of $m \to (m^*)^+$, $|m| \ll 1$, and $m \gg 1$, for different values of Pr.

4.1 Steady solution as $m \to (m^*)^+$

The behaviour of the non-dimensional skin friction coefficient $f''_{\infty}(0)$ in the vicinity of $m = m^*$, with $m > m^*$, was investigated by Hartree (1937) and the discontinuity $m = m^*$ (at which $f_{\infty}{}''(0) = 0$) was shown to be approached as $O(m - m^*)^{1/2}$. The series solutions of the ordinary differential systems (23)-(25) in powers of $(m - m^*)^{1/2}$ then provide the following expressions for the steady-state, non-dimensional skin friction coefficient and reduced surface temperature:

$$C_f(\tau)\mathrm{Re}_x^{1/2} = f''_{\infty}(0) = f^{*\prime}_{\infty,1}(0)(m - m^*)^{1/2} + O(m - m^*), \tag{26}$$

$$g_w(\tau) = g_{\infty}(0) = g^*_{\infty,0}(0) + g^*_{\infty,1}(0)(m - m^*)^{1/2} + O(m - m^*), \tag{27}$$

as $m \to (m^*)^+$ (see Harris *et al.*, (2008). As presented by Hartree (1937), the figures for the non-dimensional skin friction coefficient and the reduced surface temperature, as functions of m, for values of m close to m^* have two branches, reversed flow corresponding to points on the lower branch and arising from the negative square root in Equations (26) and (27).

4.2 Steady solution in the vicinity of $m = 0$

The solutions of the ordinary differential systems (23)-(25) in the vicinity of $m = 0$ (Blasius problem) have the following form:

$$f_{\infty}(\eta) = \sum_{i=0}^{\infty} f^0_{\infty,i}(\eta)m^i, \quad g_{\infty}(\eta) = \sum_{i=0}^{\infty} g^0_{\infty,i}(\eta)m^i. \tag{28}$$

By substituting these expressions into the systems (23)-(25) and equating coefficients of powers of m, we obtain ordinary differential systems governing the solutions for the coefficient functions $f^0_{\infty,i}(\eta)$ and $g^0_{\infty,i}(\eta)$. The first three pairs of the resulting coupled, ordinary differential systems are as follows:

$$f^{0\prime\prime\prime}_{\infty,0} + \frac{1}{2}f^0_{\infty,0}f^{0\prime\prime}_{\infty,0} = 0, \tag{29a}$$

$$\frac{1}{\mathrm{Pr}}g^{0\prime\prime}_{\infty,0} + \frac{1}{2}f^0_{\infty,0}g^{0\prime}_{\infty,0} - \frac{1}{2}f^{0\prime}_{\infty,0}g^0_{\infty,0} = 0, \tag{29b}$$

$$f^{0\prime\prime\prime}_{\infty,1} + \frac{1}{2}\left(f^0_{\infty,0}f^{0\prime\prime}_{\infty,1} + f^{0\prime\prime}_{\infty,0}f^0_{\infty,1}\right) + \frac{1}{2}f^0_{\infty,0}f^{0\prime\prime}_{\infty,0} + 1 - f^{0\prime 2}_{\infty,0} = 0, \tag{30a}$$

$$\frac{1}{\mathrm{Pr}}g^{0\prime\prime}_{\infty,1} + \frac{1}{2}\left(f^0_{\infty,0}g^{0\prime}_{\infty,1} + f^0_{\infty,1}g^{0\prime}_{\infty,0}\right) - \frac{1}{2}\left(f^{0\prime}_{\infty,0}g^0_{\infty,1} + f^{0\prime}_{\infty,1}g^0_{\infty,0}\right) + \frac{1}{2}f^0_{\infty,0}g^{0\prime}_{\infty,0} + \frac{1}{2}f^{0\prime}_{\infty,0}g^0_{\infty,0} = 0, \tag{30b}$$

$$f^{0'''}_{\infty,2}+\frac{1}{2}\left(f^{0}_{\infty,0}f^{0''}_{\infty,2}+f^{0}_{\infty,1}f^{0''}_{\infty,1}+f^{0''}_{\infty,0}f^{0}_{\infty,2}\right)+\frac{1}{2}\left(f^{0}_{\infty,0}f^{0''}_{\infty,1}+f^{0''}_{\infty,0}f^{0}_{\infty,1}\right)-2f^{0'}_{\infty,0}f^{0'}_{\infty,1}=0, \tag{31a}$$

$$\frac{1}{\mathrm{Pr}}g^{0''}_{\infty,2}+\frac{1}{2}\left(f^{0}_{\infty,0}g^{0'}_{\infty,2}+f^{0}_{\infty,1}g^{0'}_{\infty,1}+f^{0}_{\infty,2}g^{0'}_{\infty,0}\right)-\frac{1}{2}\left(f^{0'}_{\infty,0}g^{0}_{\infty,2}+f^{0'}_{\infty,1}g^{0}_{\infty,1}+f^{0'}_{\infty,2}g^{0}_{\infty,0}\right)+\frac{1}{2}\left(f^{0}_{\infty,0}g^{0'}_{\infty,1}+f^{0}_{\infty,1}g^{0'}_{\infty,0}\right)+\frac{1}{2}\left(f^{0'}_{\infty,0}g^{0}_{\infty,1}+f^{0'}_{\infty,1}g^{0}_{\infty,0}\right)=0, \tag{31b}$$

which must be solved subject to the boundary conditions:

$$f^{0}_{\infty,i}(0)=0,\quad f^{0'}_{\infty,i}(0)=0,\quad g^{0'}_{\infty,0}(0)=-1,\quad g^{0'}_{\infty,1}(0)=0,\quad g^{0'}_{\infty,2}(0)=0,\quad f^{0'}_{\infty,0}(\eta)\to 1,\quad f^{0'}_{\infty,1}(\eta)\to 0,\quad f^{0'}_{\infty,2}(\eta)\to 0,\quad g^{0}_{\infty,i}(\eta)\to 0\ \text{ as }\eta\to\infty, \tag{32}$$

for $i = 0, 1, 2$. It should be noted that the above equation satisfied by $f^{0}_{\infty,0}(\eta)$ is the well-known Blasius equation.

The steady-state non-dimensional skin friction coefficient and reduced surface temperature are given by:

$$C_f(\tau)\mathrm{Re}_x^{1/2}=f''_{\infty}(0)=f^{0''}_{\infty,0}(0)+mf^{0''}_{\infty,1}(0)+m^2f^{0''}_{\infty,2}(0)+O(m^3), \tag{33}$$

$$g_w(\tau)=g_{\infty}(0)=g^{0}_{\infty,0}(0)+mg^{0}_{\infty,1}(0)+m^2g^{0}_{\infty,2}(0)+O(m^3), \tag{34}$$

in the vicinity of $m = 0$, where:

$$f^{0''}_{\infty,0}(0)=f''_{\infty}(0)=0.3320573,\quad f^{0''}_{\infty,1}(0)=2.0029918,\quad f^{0''}_{\infty,2}(0)=-5.2648717, \tag{35}$$

and the values of $g^{0}_{\infty,0}(0), g^{0}_{\infty,1}(0)$, and $g^{0}_{\infty,2}(0)$ presented in Table I(a) have been calculated by solving the ordinary differential systems (29)-(32) using the NAG routine D02HAF for different values of Pr. These solutions are based on specifying $\eta_{\infty} = 12$, and were found to not significantly change for any larger value of η_{∞}. We notice that the value of $f''_{\infty}(0)$ coincides with that obtained by Blasius; see Lin and Lin (1987).

		Pr				
		0.72	1	2	5	10
(a)	$g^{0}_{\infty,0}(0)$	2.4397885	2.1787905	1.7207877	1.2639406	1.0021208
	$g^{0}_{\infty,1}(0)$	−3.0495140	−2.8617963	−2.4639423	−1.9682219	−1.6350249
	$g^{0}_{\infty,2}(0)$	18.9541781	17.8572698	15.5333986	12.5974804	10.5810448
(b)	$\bar{g}_{\infty,0}(0)$	0.6949205	0.5969811	0.4370114	0.2950445	0.2223738
	$\bar{g}_{\infty,1}(0)$	1.862452	1.654616	1.298038	0.9505707	0.7535070
	$\bar{g}_{\infty,2}(0)$	−1.236922	−1.096505	−0.8633464	−0.6429276	−0.5178323

Notes: (a) $g^{0}_{\infty,0}(0), g^{0}_{\infty,1}(0)$, and $g^{0}_{\infty,2}(0)$, which occur in the large-time solution (34) for the reduced surface temperature in the vicinity of $m = 0$; (b) $\bar{g}_{\infty,0}(0), \bar{g}_{\infty,1}(0)$, and $\bar{g}_{\infty,2}(0)$, which occur in the large-time solution (43) for the reduced surface temperature for $m \gg 1$

Table I.
The variations with the Prandtl number Pr

4.3 Steady solution for $m \gg 1$

For large values of m, the solutions of the differential systems (23)-(25) have the following form:

$$f_\infty(\eta) = m^{-1/2}\sum_{i=0}^{\infty}\bar{f}_{\infty,i}(\bar{\eta})m^{-i}, \quad g_\infty(\eta) = m^{1/2}\sum_{i=0}^{\infty}\bar{g}_{\infty,i}(\bar{\eta})m^{-i}, \quad \bar{\eta} = m^{1/2}\eta. \tag{36}$$

By substituting these expressions into the systems (23)-(25) and equating coefficients of powers of m, we obtain ordinary differential systems governing the solutions for the coefficient functions $\bar{f}_{\infty,i}(\bar{\eta})$ and $\bar{g}_{\infty,i}(\bar{\eta})$. The first four pairs of coupled, ordinary differential equations:

$$\bar{f}'''_{\infty,0} + \frac{1}{2}\bar{f}_{\infty,0}\bar{f}''_{\infty,0} + 1 - \bar{f}'^2_{\infty,0} = 0, \tag{37a}$$

$$\frac{1}{\mathrm{Pr}}\bar{g}''_{\infty,0} + \frac{1}{2}\left(\bar{f}_{\infty,0}\bar{g}'_{\infty,0} + \bar{f}'_{\infty,0}\bar{g}_{\infty,0}\right) = 0, \tag{37b}$$

$$\bar{f}'''_{\infty,1} + \frac{1}{2}\left(\bar{f}_{\infty,0}\bar{f}''_{\infty,0} + \bar{f}_{\infty,0}\bar{f}''_{\infty,1} + \bar{f}''_{\infty,0}\bar{f}_{\infty,1}\right) - 2\bar{f}'_{\infty,0}\bar{f}'_{\infty,1} = 0, \tag{38a}$$

$$\begin{aligned}\frac{1}{\mathrm{Pr}}\bar{g}''_{\infty,1} + \frac{1}{2}\Big(&\bar{f}_{\infty,0}\bar{g}'_{\infty,0} - \bar{f}'_{\infty,0}\bar{g}_{\infty,0} + \bar{f}_{\infty,0}\bar{g}'_{\infty,1} + \bar{f}'_{\infty,0}\bar{g}_{\infty,1}\\ &+\bar{f}_{\infty,1}\bar{g}'_{\infty,0} + \bar{f}'_{\infty,1}\bar{g}_{\infty,0}\Big) = 0,\end{aligned} \tag{38b}$$

$$\begin{aligned}\bar{f}'''_{\infty,2} + \frac{1}{2}\Big(&\bar{f}_{\infty,0}\bar{f}''_{\infty,1} + \bar{f}''_{\infty,0}\bar{f}_{\infty,1} + \bar{f}_{\infty,0}\bar{f}''_{\infty,2} + \bar{f}''_{\infty,0}\bar{f}_{\infty,2} + \bar{f}_{\infty,1}\bar{f}''_{\infty,1}\Big)\\ &- 2\bar{f}'_{\infty,0}\bar{f}'_{\infty,2} - \bar{f}'^2_{\infty,1} = 0,\end{aligned} \tag{39a}$$

$$\begin{aligned}\frac{1}{\mathrm{Pr}}\bar{g}''_{\infty,2} + \frac{1}{2}\Big(&\bar{f}_{\infty,0}\bar{g}'_{\infty,1} - \bar{f}'_{\infty,0}\bar{g}_{\infty,1} + \bar{f}_{\infty,0}\bar{g}'_{\infty,2} + \bar{f}'_{\infty,0}\bar{g}_{\infty,2} + \bar{f}_{\infty,1}\bar{g}'_{\infty,0}\\ &-\bar{f}'_{\infty,1}\bar{g}_{\infty,0} + \bar{f}_{\infty,1}\bar{g}'_{\infty,1} + \bar{f}'_{\infty,1}\bar{g}_{\infty,1} + \bar{f}_{\infty,2}\bar{g}'_{\infty,0} + \bar{f}'_{\infty,2}\bar{g}_{\infty,0}\Big) = 0,\end{aligned} \tag{39b}$$

$$\begin{aligned}\bar{f}'''_{\infty,3} + \frac{1}{2}(&\bar{f}_{\infty,0}\bar{f}''_{\infty,2} + \bar{f}''_{\infty,0}\bar{f}_{\infty,2} + \bar{f}_{\infty,0}\bar{f}''_{\infty,3} + \bar{f}''_{\infty,0}\bar{f}_{\infty,3} + \bar{f}_{\infty,1}\bar{f}''_{\infty,1} + \bar{f}_{\infty,1}\bar{f}''_{\infty,2}\\ &+\bar{f}''_{\infty,1}\bar{f}_{\infty,2}) - 2\bar{f}'_{\infty,0}\bar{f}'_{\infty,3} - 2\bar{f}'_{\infty,1}\bar{f}'_{\infty,2} = 0,\end{aligned} \tag{40a}$$

$$\begin{aligned}\frac{1}{\mathrm{Pr}}\bar{g}''_{\infty,3} + \frac{1}{2}(&\bar{f}_{\infty,0}\bar{g}'_{\infty,2} - \bar{f}'_{\infty,0}\bar{g}_{\infty,2} + \bar{f}_{\infty,0}\bar{g}'_{\infty,3} + \bar{f}'_{\infty,0}\bar{g}_{\infty,3}\\ &+\bar{f}_{\infty,1}\bar{g}'_{\infty,1} - \bar{f}'_{\infty,1}\bar{g}_{\infty,1} + \bar{f}_{\infty,1}\bar{g}'_{\infty,2}\\ &+\bar{f}'_{\infty,1}\bar{g}_{\infty,2} + \bar{f}_{\infty,2}\bar{g}'_{\infty,0} - \bar{f}'_{\infty,2}\bar{g}_{\infty,0} + \bar{f}_{\infty,2}\bar{g}'_{\infty,1}\\ &+\bar{f}'_{\infty,2}\bar{g}_{\infty,1} + \bar{f}_{\infty,3}\bar{g}'_{\infty,0} + \bar{f}'_{\infty,3}\bar{g}_{\infty,0}) = 0,\end{aligned} \tag{40b}$$

where primes denote differentiation with respect to $\bar{\eta}$, must be solved subject to the boundary conditions:

$$\begin{aligned} &\bar{f}_{\infty,i}(0) = 0, \quad \bar{f}'_{\infty,i}(0) = 0, \quad \bar{g}'_{\infty,0}(0) = 0, \quad \bar{g}'_{\infty,1}(0) = -1, \\ &\qquad \bar{g}'_{\infty,2}(0) = 0, \quad \bar{g}'_{\infty,3}(0) = 0, \\ &\bar{f}'_{\infty,0}(\bar{\eta}) \to 1, \quad \bar{f}'_{\infty,1}(\bar{\eta}) \to 1, \quad \bar{f}'_{\infty,2}(\bar{\eta}) \to 1, \quad \bar{f}'_{\infty,3}(\bar{\eta}) \to 1, \\ &\qquad \bar{g}_{\infty,i}(\bar{\eta}) \to 0 \quad \text{as} \quad \bar{\eta} \to \infty, \end{aligned} \tag{41}$$

for $i = 0, 1, 2, 3$.

The above ordinary differential Equation (37b), subject to the associated boundary conditions (41), comprising the problem for $\bar{g}_{\infty,0}(\bar{\eta})$ clearly has an infinite family of solutions, since if $\bar{g}_{\infty,0}(\bar{\eta})$ is one solution then so is $\bar{a}\bar{g}_{\infty,0}(\bar{\eta})$, where $\bar{a}$ is an arbitrary constant. In a similar manner to the problem described in section 4.1, by additionally requiring that the ordinary differential system (38) subject to its associated boundary conditions (41) is soluble, a unique solution for $\bar{g}_{\infty,0}(\bar{\eta})$ can be achieved, although the resulting solution for $\bar{g}_{\infty,1}(\bar{\eta})$ will not be valid. The NAG routine D02HAF can now be used to solve the ordinary differential systems (37)-(41), although the solutions for $\bar{g}_{\infty,3}(\bar{\eta})$ will not be valid.

The steady-state non-dimensional skin friction coefficient and the reduced wall temperature are given by:

$$\begin{aligned} C_f(\tau)\mathrm{Re}_x^{1/2} = \left.\frac{\mathrm{d}^2 f_\infty(\eta)}{\mathrm{d}\eta^2}\right|_{\eta=0} &= m^{1/2}\bar{f}''_{\infty,0}(0) + m^{-1/2}\bar{f}''_{\infty,1}(0) \\ &\quad + m^{-3/2}\bar{f}''_{\infty,2}(0) + O\left(m^{-5/2}\right), \end{aligned} \tag{42}$$

$$\begin{aligned} g_w(\tau) = g_\infty(0) &= m^{1/2}\bar{g}_{\infty,0}(0) + m^{-1/2}\bar{g}_{\infty,1}(0) \\ &\quad + m^{-3/2}\bar{g}_{\infty,2}(0) + O\left(m^{-5/2}\right), \end{aligned} \tag{43}$$

for $m \gg 1$, where:

$$\bar{f}''_{\infty,0}(0) = 1.1930434, \quad \bar{f}''_{\infty,1}(0) = 0.0391436, \quad \bar{f}''_{\infty,2}(0) = 0.0005789, \tag{44}$$

and the values of $\bar{g}_{\infty,0}(0), \bar{g}_{\infty,1}(0)$, and $\bar{g}_{\infty,2}(0)$ are presented in Table I(b) for different values of Pr. These solutions are based on specifying $\bar{\eta}_\infty \approx$ 9-13 (dependent on the value of Pr), and were found to not significantly change for any larger value of $\bar{\eta}_\infty$.

4.4 Steady solution for $m^* \leq m < \infty$

To describe the large-time, steady-state solution to the transient heat transfer problem described in this paper, we are mainly concerned with the Blasius-like solutions to the system (23)-(25). As explained in this section, such solutions exist for $m^* \leq m < \infty$ and the NAG routine D02HAF can be employed to numerically determine the complete behaviour of the non-dimensional skin friction coefficient and the reduced surface temperature over this range. These Blasius-like numerical solutions, together with the solutions exhibiting regions of reversed flow near to the surface, are compared to the various asymptotic behaviours derived in sections 4.1-4.3 in Figure 2, for different values of the Prandtl number Pr. The value of η_∞ at which the boundary conditions

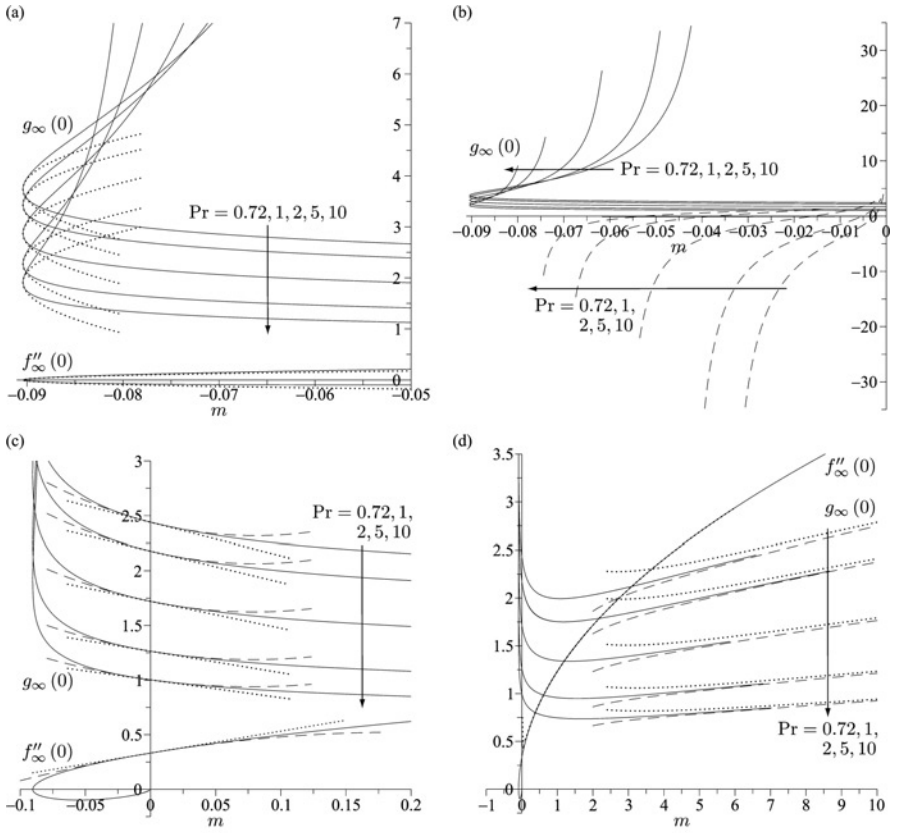

Notes: (a) Close to the value $m = m^*$, with the dotted line representing the $m \to (m^*)^+$ solutions (26) and (27); (b) over the range $m^* \leq m \leq 0$, with the dashed lines showing the second branch of $g_\infty(0)$ corresponding to reversed flow cases (the $f''_\infty(0)$ variation has not been presented for clarity); (c) in the vicinity of $m = 0$, with the dotted and dashed lines representing the two- and three-term, respectively, approximations (33) and (34); and (d) for large values of m, with the dotted and dashed lines representing the two- and three-term, respectively, approximations (42) and (43)

Figure 2.
The variation of $f''_\infty(0)$ with m, and $g_\infty(0)$ with m at different values of Pr

(25) that are valid as $\eta \to \infty$ are to be applied depends crucially upon the chosen value of m, particularly near to m^* and for the reversed flow cases.

Figure 2(a) shows the behaviour of $f''_\infty(0)$ and g_∞ (0) as $m \to (m^*)^+$, where m^* defines the point at which the boundary layer breaks away from the surface. As discussed in section 4.1, the numerical solutions for $m^* < m < 0$ have two branches, the reversed flow solutions corresponding to those branches existing over the range $m^* < m < 0$ only. As in similar physical situations, we postulate that the upper branch solutions are physically stable and occur in practice, whilst the lower branch solutions are not physically obtained. This postulate can be verified by performing a stability analysis but this is beyond the scope of the present paper. The expansions (26) and (27) are valid as $m \to (m^*)^+$ and have been presented in Figure 2(a) using the first two terms, namely the terms up to $O(m - m^*)^{1/2}$, with the term of $O(m - m^*)^0$ in

Equation (26) being identically zero. The two-term approximations are only valid over a very small interval of m values as $m \to (m^*)^+$.

For all values of the Prandtl number, Pr, the value of $g_\infty(0)$ rapidly increases along the upper branch of the solution curves shown in Figure 2(a), and this rapid increase occurs nearer to m^* as Pr increases. Corresponding to the remainder of the displayed reversed flow solution branch for $f''_\infty(0)$ over $m^* < m < 0$, a further branch of solutions for $g_\infty(0)$ exists. This branch of solutions for $g_\infty(0)$ has only been displayed in Figure 2(b), together with the other solutions over the range $m^* < m < 0$. The majority of this branch of solutions correspond to the interesting cases in which the surface temperature is negative, but all are characterised by the existence of a negative temperature somewhere within the fluid.

Figure 2(c) shows the variation of $f''_\infty(0)$ and $g_\infty(0)$ in the vicinity of $m = 0$ in comparison to the two- and three-term expansions (33) and (34). The three-term, quadratic approximations to the behaviour of $f''_\infty(0)$ and $g_\infty(0)$ are only graphically indistinguishable from the corresponding numerical solutions over the interval $|m| \lesssim 0.035$, although they slightly extend the range of validity of the linear two-term approximations.

Figure 2(d) shows the variations of $f''_\infty(0)$ and $g_\infty(0)$ at large values of m in comparison to the two- and three-term large-m expansions presented in Equations (42) and (43) for the non-dimensional skin friction coefficient and the reduced surface temperature, respectively. It should be noted that the one-term solutions provide a reasonable approximation to $f''_\infty(0)$ for $m \geq 5$, but are relatively poor for the displayed interval of m values when the $g_\infty(0)$ solution is considered. A significant improvement in the validity of the large-m approximation is observed when the second and third terms in each expansion are included. In the approximation for $f'_\infty(0)$, the two- and three-term expansions (42) are graphically indistinguishable from the corresponding numerical solution for $m \gtrsim 0.25$. In the approximation for $g_\infty(0)$, the three-term expansion (43) provides a graphically accurate representation for $m \gtrsim 8$, and again provides a better approximation than the two-term expansion.

4.5 Large-time fluid velocity and temperature profiles

The large-time, steady-state profiles of the non-dimensional fluid velocity function $f''_\infty(\eta)$ and the fluid temperature function $g_\infty(\eta)$ are presented in Figures 3 and 4 for different values of m and Pr. The Blasius-like numerical solutions to Equations (23)-(25) have been presented in Harris *et al.* (2008) for a variety of values of m over the range $m^* \leq m \leq 2$, and the effect on the steady-state fluid temperature profiles of changing Pr from 1 to 10 has been considered. The effect of varying Pr, at a constant value of m, is further illustrated in Figure 4. The reversed flow cases are shown in Figure 3 for four values of m within the range $m^* < m < 0$. For the reversed flow cases, there is a significant increase in both the thermal and the velocity boundary-layer thicknesses, and the value of η_∞ must accordingly be increased when calculating such numerical solutions. Three distinct types of non-dimensional fluid temperature profile exist, all of which maintain the boundary condition $g'_\infty(0) = -1$. Firstly, for the reversed flow cases corresponding to the upper solution branches in Figure 2(a) that exist for a small range of values of $m > m^*$, solutions for $g_\infty(\eta)$ exist in which the fluid temperature is positive for all values of η and monotonically decreases with η through the thermal boundary layer. However, the surface temperature rapidly increases with m until the further branch of solutions presented in Figure 2(b) is reached. The second type of non-dimensional fluid temperature profile is now obtained, and these correspond to cases in

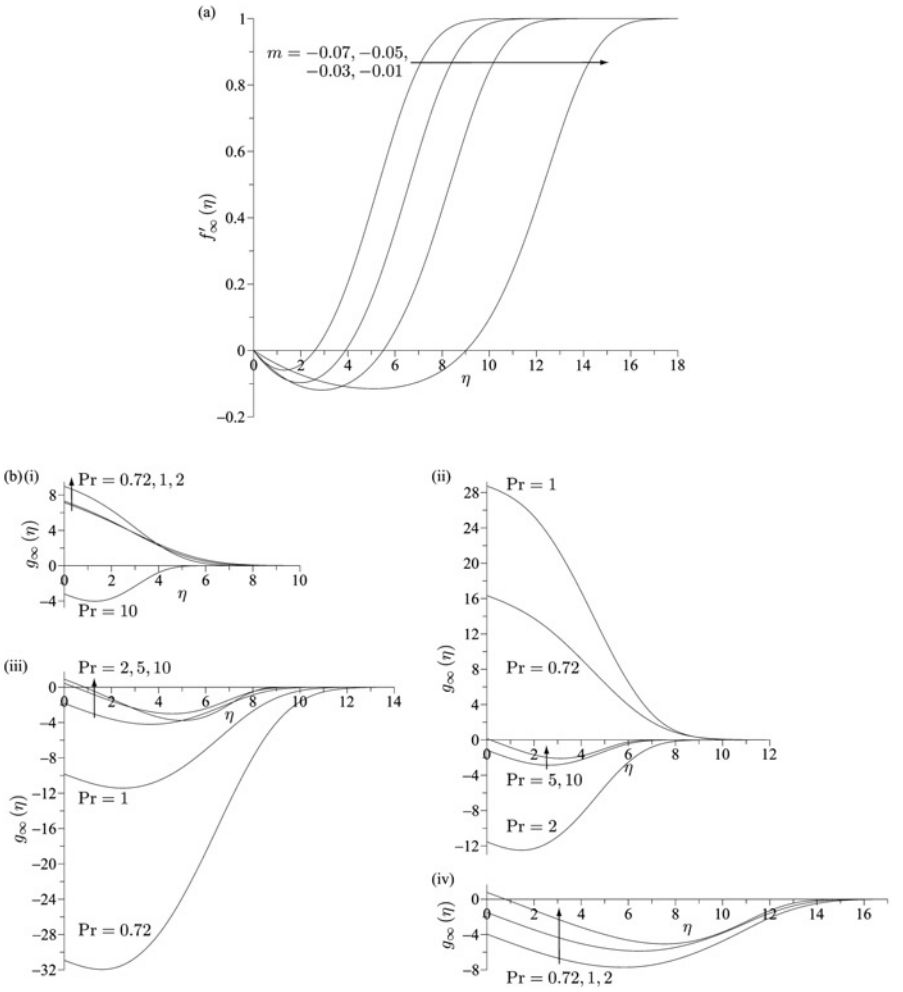

Figure 3.
Large-time, steady-state, non-dimensional

Notes: The curves for Pr = 5 when m = –0.07, and Pr = 5 and 10 when m = –0.01 could not be calculated as these lie in the region between the two branches of the reversed flow solutions presented in Figure 2(b)

which the surface temperature is negative and the fluid temperature is negative for all values of η. Due to the boundary condition at the surface, a local minimum in the fluid temperature occurs within the fluid. Finally, as m continues to increase, the surface temperature becomes positive, and there is a region close to the surface within which the fluid temperature remains positive.

The Blasius-like, large-time, steady-state profiles of the non-dimensional fluid temperature $g_\infty(\eta)$ are presented in Figures 4(a)-(c) for $m = m^*, m = 1/5$, and $m = 2$, respectively, at the five values of Pr $= 0.72$, 1, 2, 5, and 10. Figure 4 demonstrates that an increase in the value of Pr leads to a reduction in the surface temperature and, as expected, a decrease in the thermal boundary-layer thickness. For the Blasius-like

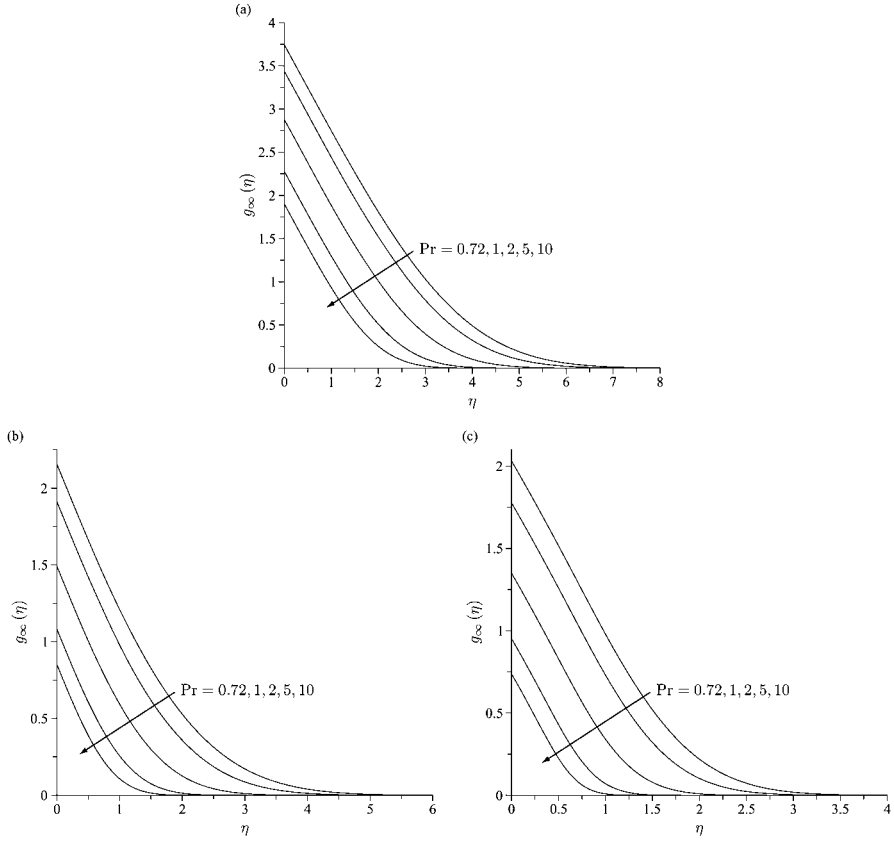

Notes: (a) $m = m^*$; (b) $m = 1/5$; (c) $m = 2$

Figure 4.
Large-time, steady-state, non-dimensional fluid temperature $g_\infty(\eta)$ profiles at different values of Pr

solutions, the corresponding non-dimensional fluid temperature profiles for other values of m show the same tendencies and, therefore, have not been presented here.

5. Numerical solutions

Initially the transient effects due to the imposition of a constant heat flux at the surface are confined to a thin fluid region near to the surface and are described by the small-time solution developed in section 3. These effects continue to penetrate outward through the initial boundary layer and ultimately evolve into a steady-state flow. In order to match these small- and large-time solutions, we now develop a numerical solution of the governing boundary-layer Equations (4)-(6).

The evolution of the pairs of functions $\partial F/\partial\zeta, G$ and $\partial f/\partial\eta, g$ are separately governed by the pairs of coupled partial differential Equations (15), (16) and (9), (10), respectively, which are each parabolic and thus can be integrated numerically using a step-by-step method similar to that described by Merkin (1972), provided that the coefficients of $\partial^2 F/\partial\zeta\partial\tau$, $\partial G/\partial\tau$, $\partial^2 f/\partial\eta\partial\tau$, and $\partial g/\partial\tau$ remain positive throughout the solution domain. This marching method enables the solution at time $\tau = 0$, described by the functions:

$$F_0'(\zeta) = \operatorname{erf}\zeta,$$
$$G_0(\zeta) = -\zeta\,\operatorname{erfc}\left(\sqrt{\Pr}\,\zeta\right) + \frac{1}{\sqrt{\pi \Pr}}\,e^{-\Pr\zeta^2} \tag{45}$$

obtained from the analytical solutions to the first ordinary differential system associated with the expansion (18), for $\zeta \geq 0$, to proceed in time. For $m \geq 1$, this forward integration can be continued toward the steady-state solution profiles. However, for $m < 1$, the marching method only provides a numerical solution for $\tau \leq \tau_n^*$, where τ_n^* is the time at which the above-mentioned coefficients first become negative in the numerical procedure. The value of τ_n^* will be approximately equal to the precise time τ_p^* at which these coefficients first change sign at the outer edge of the boundary layer, namely:

$$\tau_n^* \approx \tau_p^* = \frac{1}{1-m}, \tag{46}$$

for $m < 1$. Physically, as well as mathematically, when $m < 1$ we would expect that $\tau_n^* = 1/(1-m)$, since for $\tau < 1/(1-m)$ the disturbance from the leading edge has not been felt. The disturbance travels fastest at the outer edge of the boundary layer and, therefore, it is first encountered at such locations when $\tau = 1/(1-m)$.

The application of the step-by-step scheme to Equations (15) and (16) enables the accurate evolution of the fluid temperature and velocity profiles to be determined over a developing boundary layer whose width increases with time. If ζ_∞ and η_∞ are interpreted as being finite values of the spatial variables at which the associated boundary conditions are to be applied, then at the exact time $\tilde{\tau}_p = (\eta_\infty/2\zeta_\infty)^2$ we must transfer to the step-by-step scheme applied to Equations (9) and (10). We again adopt the notation $\tilde{\tau}_n$ to denote the corresponding value of τ that is actually reached in our numerical techniques.

In order to accurately evaluate the initial evolution of the non-dimensional fluid velocity function $\Phi(\zeta, \tau) = \partial F/\partial\zeta(\zeta, \tau)$ and the fluid temperature function $G(\zeta, \tau)$ we apply the direct, forward-integration scheme to the integro-differential form of Equations (15) and (16), following the formulation described in Harris *et al.* (1997b, 1998, 1999, 2001, 2002). The finite spatial domain is divided into N^ζ equal grid spacings of length $h^\zeta = \zeta_\infty/N^\zeta$ and a variable time step is used. To accurately describe the initial evolution, the time increment $\Delta\tau_0$ at time $\tau = 0$ is set to some prescribed small value and subsequently a time step doubling procedure is adopted to reduce the computations at later times. Based upon the fluid velocity and temperature profiles at the final time $\tilde{\tau}_n$ reached in this numerical scheme, we now apply the step-by-step method to Equations (9) and (10) and continue toward the steady-state solution or the time $\tau_p^* = 1/(1-m)$, according as to whether $m \geq 1$ or $m < 1$, respectively. The numerical formulation used in the papers by Harris *et al.* (1997b, 1998, 1999, 2001, 2002) is employed, based upon N^η equal grid spacings for the spatial discretisation.

In the cases for which $m < 1$, at the time $\tau = \tau_n^*$ the forward-integration approach breaks down and the coefficients of $\partial^2 f/\partial\eta\partial\tau$ and $\partial g/\partial\tau$ in the governing Equations (9) and (10), respectively, are tending toward negative values as $\eta \to \infty$. Based upon the profiles $\partial f/\partial\eta(\eta, \tau_n^*)$ and $g(\eta, \tau_n^*)$ at this time and the asymptotic steady-state profiles $f_\infty(\eta)$, $f_\infty'(\eta)$, and $g_\infty(\eta)$, defined as the solution of the system of Equations (23)-(25), we complete the numerical integration and derive a solution over $\tau_n^* < \tau < \infty$ by adopting a matching approach. The matching technique originated by Dennis

(1972) has been successfully applied by the present authors to some related heat transfer problems; see Harris *et al.* (1997a,b, 1998, 1999, 2001, 2002), wherein comprehensive details of this iterative approach are presented. In the finite-difference approximation to Equations (9) and (10), we replace the time derivatives within the terms $\partial^2 f/\partial\eta\partial\tau$ and $\partial g/\partial\tau$ by either a backward or forward difference, depending on whether their coefficient $1 + (m-1)\tau\partial f/\partial\eta$ is positive or negative, respectively, to achieve a convergent solution using standard iterative techniques. At some large, but finite, time $\tau = \tau_\infty$ the solution is given by the steady-state analysis. The value of τ_∞ may be varied, but must be taken to be large enough for any further increase to have a negligible effect on the whole solution for $\tau_n^* < \tau < \tau_\infty$.

6. Results and discussion

In the discussion of the parameters within the numerical procedures for determining the transient fluid velocity and temperature fields that follows, we illustrate the results obtained by concentrating mainly on the case when the Prandtl number $\mathrm{Pr} = 1$ and $m = 1/5$, namely a wedge angle of 60°. Required alterations to these parameters are then discussed with reference to variations in Pr and m separately.

6.1 Results for Pr = 1 and m = 1/5

The restriction to a finite-dimensional ζ space was achieved by taking $\zeta_\infty = 8$ for $\mathrm{Pr} = 1$ and $m = 1/5$, and thus the precise time at which the transfer to the step-by-step method in η, τ variable takes place is $\tilde{\tau}_p = 0.5625$, taking $\eta_\infty = 12$. The effect on the forward-integration numerical schemes of increasing the values of ζ_∞ and η_∞, whilst keeping the corresponding spatial mesh sizes h^ζ and h^η, respectively, constant, was investigated and it was concluded that the results for the non-dimensional fluid velocity and temperature profiles, together with the evolution of the non-dimensional skin friction coefficient, were graphically indistinguishable from those presented in the figures within this paper.

The first time increment $\Delta\tau_0$ was assigned the value $\Delta\tau_0 = 10^{-10}$ and the adopted time step doubling procedure was successful in increasing this time step (or any smaller initial time step) to $\Delta\tau = O(10^{-5})$ at the non-dimensional time $\tau_n^* \approx 1.25$, namely the time of termination of the forward-integrating procedure, over the complete range of spatial grid sizes described below. The numerical value of $\eta_\infty = 2\zeta_\infty \tilde{\tau}_n^{1/2} = 11.99981$ was obtained, based upon the time $\tilde{\tau}_n = 0.56248$ of transfer between the step-by-step methods in the ζ, τ and η, τ variables.

The most significant source of variation in the numerical solutions for the non-dimensional fluid velocity function $\partial f/\partial\eta(\eta,\tau) = \partial F/\partial\zeta(\zeta(\eta,\tau),\tau)$ and the fluid temperature function $g(\eta,\tau) = G(\zeta(\eta,\tau),\tau)$ arise by considering changes in the number of grid spaces N^ζ and N^η associated with the step-by-step methods in the ζ, τ and η, τ variables, respectively. In Tables II(a) and (b) we present both the numerical solutions (see section 5) and the small-time approximations (21) for the non-dimensional skin friction coefficient $C_f(\tau)\mathrm{Re}_x^{1/2}$ and reduced surface temperature $g_w(\tau)$, respectively, in the case of $\mathrm{Pr} = 1$ and $m = 1/5$, with some of the results in Table II(a) being in accordance with those presented in Harris *et al.* (2002). These tables illustrate the effect of refining the spatial grid from $N = N^\zeta = N^\eta = 100$ to 6,400 grid spaces, corresponding to reducing $h^\zeta = 2/3h^\eta = 0.08$ to $h^\zeta = 2/3h^\eta = 0.00125$, by repeatedly doubling the value of N. It is observed that, as N increases, the initial development of the numerical solution approaches that of the appropriate small-time solution.

Table II.

τ	N 100	200	400	800	1,600	3,200	6,400	Small-τ solution One term	Two terms	Three terms
(a)										
0.00001	179.403912	178.662186	178.475332	178.428529	178.416823	178.413896	178.413164	178.412414	178.412922	178.412922
0.0001	56.733940	56.499389	56.440302	56.425502	56.421800	56.420874	56.420643	56.418959	56.420566	56.420566
0.0004	28.369370	28.252103	28.222561	28.215162	28.213311	28.212848	28.212732	28.209480	28.212694	28.212694
0.001	17.945402	17.871245	17.852564	17.847884	17.846714	17.846421	17.846348	17.841241	17.846323	17.846323
0.004	8.980292	8.943239	8.933904	8.931566	8.930981	8.930835	8.930798	8.920620	8.930786	8.930785
0.01	5.689238	5.665835	5.659939	5.658462	5.658092	5.658000	5.657977	5.641896	5.657969	5.657967
0.04	2.868628	2.857005	2.854076	2.853342	2.853158	2.853112	2.853101	2.820948	2.853094	2.853084
0.1	1.844659	1.837407	1.835578	1.835120	1.835005	1.834976	1.834969	1.784124	1.834951	1.834912
0.2	1.340201	1.335188	1.333922	1.333605	1.333525	1.333505	1.333500	1.261566	1.333446	1.333337
0.3	1.123560	1.119559	1.118548	1.118294	1.118230	1.118215	1.118211	1.030065	1.118099	1.117898
0.4	0.998438	0.995051	0.994193	0.993978	0.993924	0.993911	0.993908	0.892062	0.993715	0.993406
0.6	0.856698	0.854156	0.853513	0.853351	0.853311	0.853301	0.853298	0.728366	0.852865	0.852297
0.8	0.777589	0.775907	0.775483	0.775377	0.775350	0.775344	0.775342	0.630783	0.774542	0.773668
1.2	0.694229	0.693400	0.693192	0.693140	0.693127	0.693124	0.693123	0.515032	0.691101	0.689495
1.8 (τ_∞=5)	0.642473	0.642139	0.642057	0.642036	0.642031	0.642032	–			
1.8 ($\tau_\infty = 8$)	0.642473	0.642139	0.642057	0.642036	0.642031	0.642032	–			
2.4 ($\tau_\infty = 5$)	0.625741	0.625604	0.625572	0.625564	0.625563	0.625565	–			
2.4 ($\tau_\infty = 8$)	0.625743	0.625604	0.625572	0.625564	0.625563	0.625565	–			
4.8 ($\tau_\infty = 5$)	0.621306	0.621316	0.621321	0.621323	0.621324	0.621326	–			
4.8 ($\tau_\infty = 8$)	0.621383	0.621335	0.621326	0.621324	0.621324	0.621327	–			
6.4 ($\tau_\infty = 8$)	0.621338	0.621324	0.621323	0.621324	0.621324	0.621326	–	Steady state:		0.621324
(b)										
0.00001	0.003565	0.003568	0.003568	0.003568	0.003568	0.003568	0.003568	0.003568	0.003568	0.003568
0.0001	0.011275	0.011282	0.011283	0.011284	0.011284	0.011284	0.011284	0.011284	0.011284	0.011284
0.0004	0.022549	0.022563	0.022566	0.022567	0.022567	0.022567	0.022568	0.022568	0.022568	0.022568
0.001	0.035654	0.035675	0.035680	0.035682	0.035682	0.035682	0.035682	0.035682	0.035682	0.035682
0.004	0.071306	0.071348	0.071359	0.071362	0.071362	0.071363	0.071363	0.071365	0.071363	0.071363

(*continued*)

τ	N						Small-τ solution		
	100	200	400	800	1,600	3,200	6,400	One term	Two terms	Three terms
0.01	0.112739	0.112806	0.112823	0.112827	0.112828	0.112829	0.112829	0.112838	0.112829	0.112829
0.04	0.225422	0.225558	0.225592	0.225600	0.225602	0.225603	0.225603	0.225676	0.225602	0.225603
0.1	0.356254	0.356468	0.356521	0.356535	0.356538	0.356539	0.356539	0.356825	0.356534	0.356539
0.2	0.503429	0.503732	0.503808	0.503827	0.503831	0.503832	0.503833	0.504627	0.503805	0.503832
0.3	0.616113	0.616483	0.616576	0.616599	0.616605	0.616607	0.616607	0.618039	0.616530	0.616605
0.4	0.710915	0.711344	0.711451	0.711478	0.711485	0.711487	0.711487	0.713650	0.711327	0.711480
0.6	0.869528	0.870052	0.870183	0.870216	0.870224	0.870226	0.870227	0.874039	0.869771	0.870194
0.8	1.002933	1.003474	1.003609	1.003643	1.003652	1.003654	1.003654	1.009253	1.002683	1.003551
1.2	1.226316	1.226816	1.226941	1.226972	1.226980	1.226982	1.226983	1.236077	1.224007	1.226400
1.8 ($\tau_\infty = 5$)	1.501706	1.502145	1.502255	1.502282	1.502287	1.502284	–			
1.8 ($\tau_\infty = 8$)	1.501706	1.502145	1.502255	1.502282	1.502286	1.502280	–			
2.4 ($\tau_\infty = 5$)	1.720107	1.720383	1.720450	1.720462	1.720446	1.720364	–			
2.4 ($\tau_\infty = 8$)	1.720106	1.720383	1.720449	1.720458	1.720429	1.720303	–			
4.8 ($\tau_\infty = 5$)	1.912006	1.911054	1.910815	1.910752	1.910721	1.910656	–			
4.8 ($\tau_\infty = 8$)	1.912077	1.911070	1.910816	1.910744	1.910687	1.910504	–			
6.4 ($\tau_\infty = 8$)	1.912160	1.911146	1.910893	1.910829	1.910813	1.910806	–	Steady state:		1.910808

Notes: Values of (a) non-dimensional skin friction coefficient $C_f(\tau)\mathrm{Re}_x^{1/2} = \partial^2 f/\partial\eta^2(0,\tau)$; (b) reduced surface temperature $g_w(\tau) = g(0,\tau)$ when $\mathrm{Pr} = 1$, for the case $m = 1/5$, obtained using different spatial grid sizes $N = N^\zeta = N^\eta$, in comparison to the small-time solution (21)

Table II.

Table II also includes results obtained from the matching numerical procedure, for which the value of $\eta_\infty \approx 12$ is maintained, a value which has been shown to be both valid for $\tau \leq \tau_n^*$ and as $\tau \to \infty$. The restriction to a finite temporal domain requires that the final, steady-state profiles be enforced at the finite value $\tau = \tau_\infty$, corresponding to $\tau \to \infty$. The solutions for the non-dimensional skin friction coefficient and the reduced surface temperature have been observed to smoothly approach their steady-state solutions when τ_∞ is imposed at $\tau_\infty = 8$, for $\Pr = 1$ and $m = 1/5$, with no significant improvement in accuracy when τ_∞ is extended beyond this value. This fact is further demonstrated in Table II by the very close agreement between the matching solutions achieved using $\tau_\infty = 5$ and 8. The temporal domain from the time of termination τ_n^* of the forward-integrating approach to τ_∞ is divided into 992 and 1,786 increments for $\tau_\infty = 5$ and 8, respectively, both corresponding to a time step of approximately 0.00378. For the finest spatial grids, computational limitations make the investigation of finer temporal grids a very time consuming process, and the use of more than 1,786 temporal grid increments for a spatial grid of $N = 1{,}600$ when $\tau_\infty = 8$ is believed to provide results that will be graphically indistinguishable from those achieved with such a discretisation. The convergence of the iterative scheme is described by the approach of the average absolute error over the solution domain to a specified error tolerance. Due to the slow convergence of this numerical procedure, the error tolerance is made small, namely 5×10^{-10}, and the solutions produced by more restrictive tolerances are graphically indistinguishable from those presented here.

For the example of $\Pr = 1$ and $m = 1/5$ shown in Table II, the times at which the third term in the small-time solution (21) begins to influence the result presented are $\tau = 0.01$ and 0.04 for the non-dimensional skin friction coefficient and reduced surface temperature, respectively, while the times at which these small-time approximations begin to become invalid are around $\tau = 0.1$ and 0.6, respectively.

Table II demonstrates that, at later times in the transient process, the differences in the results obtained using the different spatial grids are less significant. The solutions achieved using all of these grids are almost graphically indistinguishable at any time value through the transient process. For all but the coarsest spatial grids, the solutions are all seen to smoothly approach the predicted steady-state value of the non-dimensional skin friction coefficient, both for $\tau_\infty = 5$ and 8, with the extension of τ_∞ beyond 5 having almost no effect on these matching numerical solutions. Note that the matching solution was not calculated for $n = 6{,}400$ as it was computationally very expensive. However, for the non-dimensional reduced surface temperature, the extension of τ_∞ from 5 to 8 has a more significant influence, and this latter value of $\tau_\infty = 8$ has therefore been used for the figures presented in this paper for $\Pr = 1$ and $m = 1/5$.

The slight improvement in the accuracy that is achieved as N increases from $N = 1{,}600$ to 3,200 and 6,400 is not justified by the additional computational time required. The efficiency of this numerical procedure enables solutions to be achieved relatively rapidly using $h^\zeta = 2/3h^\eta = 0.005$, and, therefore, this value has been used for all of the remaining results presented in this paper, so that $N = 1{,}600$.

Figures 5(a) and 6(a) show the variation of the non-dimensional fluid velocity $\partial f/\partial\eta(\eta, \tau)$ and the non-dimensional fluid temperature $g(\eta, \tau)$ profiles, respectively, at various times τ through the transient process, calculated for $\Pr = 1$ and $m = 1/5$. The analytical expressions for the small-time solutions, namely the first two terms in Equations (19) and (20), have been included in these figures for the time periods over

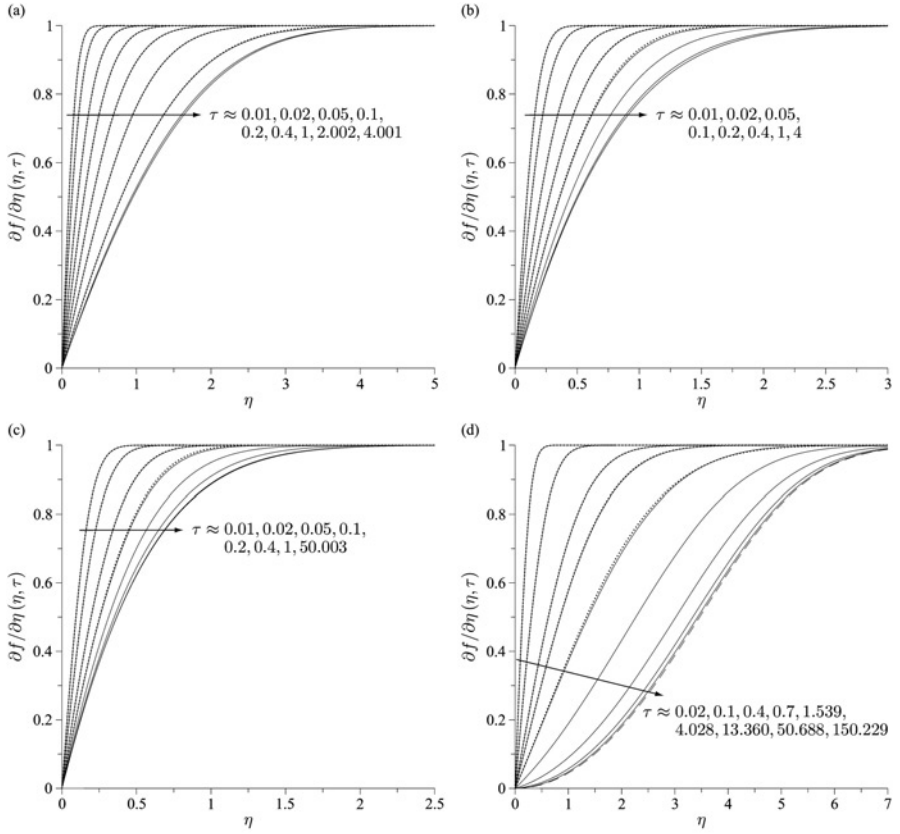

Notes: The first two terms (up to $O(\tau)$) in the small-time profiles (19) are represented by dotted lines for the times at which they remain accurate, namely the first (a) 7, (b) 5, (c) 4, and (d) 5 of the indicated times. The ultimate steady-state solution of the system (23)-(25) is represented by dashed line; (a) $m = 1/5$; (b) $m = 1$; (c) $m = 2$; (d) $m = m^*$

Figure 5.
The profiles of the non-dimensional fluid velocity $\partial f/\partial \eta(\eta, \tau)$ at different values of the non-dimensional time τ

which they provide a good approximation to the numerical solutions, and for the case of $\mathrm{Pr} = 1$ and $m = 1/5$ these approximations remain valid up to $\tau \approx 2$. The final, steady-state profiles, as predicted by Equations (23)-(25), are also included in Figures 5(a) and 6(a), and the numerical profiles evolve monotonically from $\tau = 0$ toward these steady-state profiles.

Figures 7 and 8 show the evolution of the non-dimensional skin friction coefficient $C_f(\tau)\mathrm{Re}_x^{1/2}$ and the reduced surface temperature $g_w(\tau)$, respectively, for the case of $\mathrm{Pr} = 1$ and $m = 1/5$. The numerical, transient solutions are shown in Figures 7(a) and 8(a) to develop closely following the small-time solution (21), and both the two- and three-term solutions are almost graphically identical to the numerical solutions for $\tau \lesssim 1.15$, as is expected from the results presented in Table II. The one-term, small-time solutions provide an accurate approximation to the numerical solutions only over a relatively limited initial time interval. The transient, numerical solutions for $C_f(\tau)\mathrm{Re}_x^{1/2}$ and $g_w(\tau)$ determined using the matching method, continuing from the forward-integrating solution, have also been included in Figures 7 and 8, respectively. In

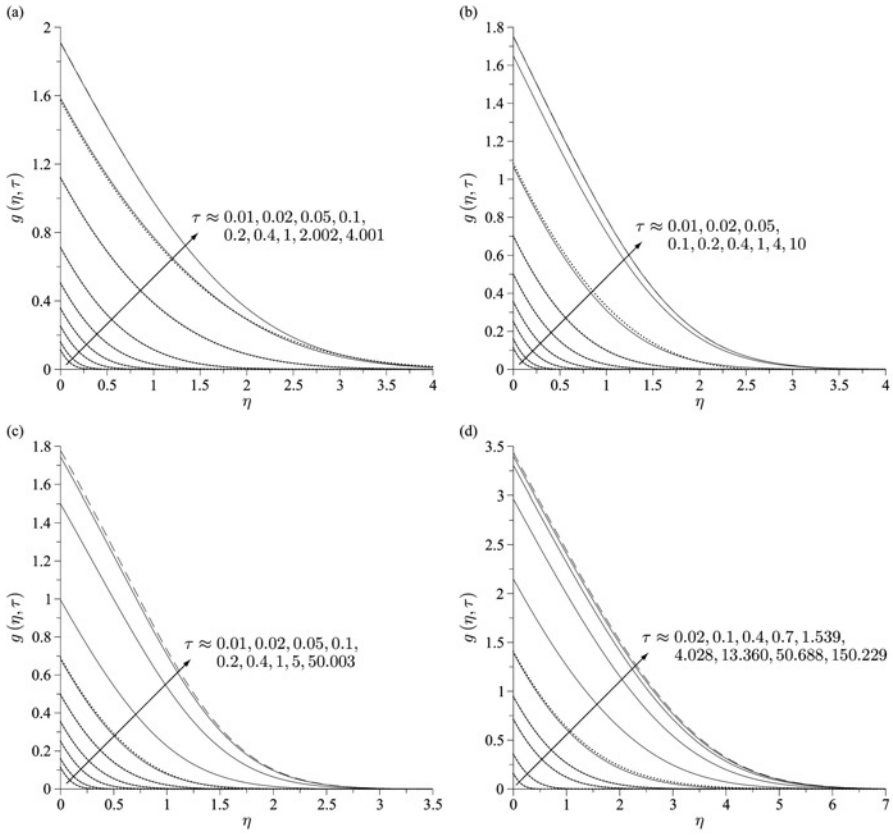

Figure 6.
The profiles of the non-dimensional fluid temperature $g(\eta, \tau)$ at different values of the non-dimensional time τ

Notes: The first two terms (up to $O(\tau^{3/2})$) in the small-time profiles (20) are represented by dotted lines for the times at which they remain accurate, namely the first (a) 8, (b) 7, (c) 6, and (d) 5 of the indicated times. The ultimate steady-state solution of the system (23)-(25) is represented by dashed line; (a) $m = 1/5$; (b) $m = 1$; (c) $m = 2$; (d) $m = m^*$

addition, Figures 7(b) and 8(b) display the approach of the transient, numerical solutions toward the corresponding large-time, steady-state value predicted in Table III(a). For the case of $\mathrm{Pr} = 1$ and $m = 1/5$, the solutions for the non-dimensional skin friction coefficient and the reduced surface temperature approximately reach their steady-state values at $\tau \approx 2.5$ for $C_f(\tau)\mathrm{Re}_x^{1/2}$ and $\tau \approx 4$ for $g_w(\tau)$, from a graphical viewpoint. The three-term small-time solutions are again included in Figures 7(b) and 8(b) to further demonstrate the ranges over which the initial and final asymptotic solutions can be applied. It should be noted that Figures 7(b) and 8(b) have been presented using a logarithmic horizontal axis to enable the solutions discussed in section 6.2 to be directly compared.

Finally, in order to be applicable to practical engineering problems, we consider the simple matching solution developed by Harris *et al.* (2002) for the non-dimensional skin friction coefficient. Although these matching solutions are not unique, it is sometimes convenient, for engineering purposes, to seek a closed form approximate solution that

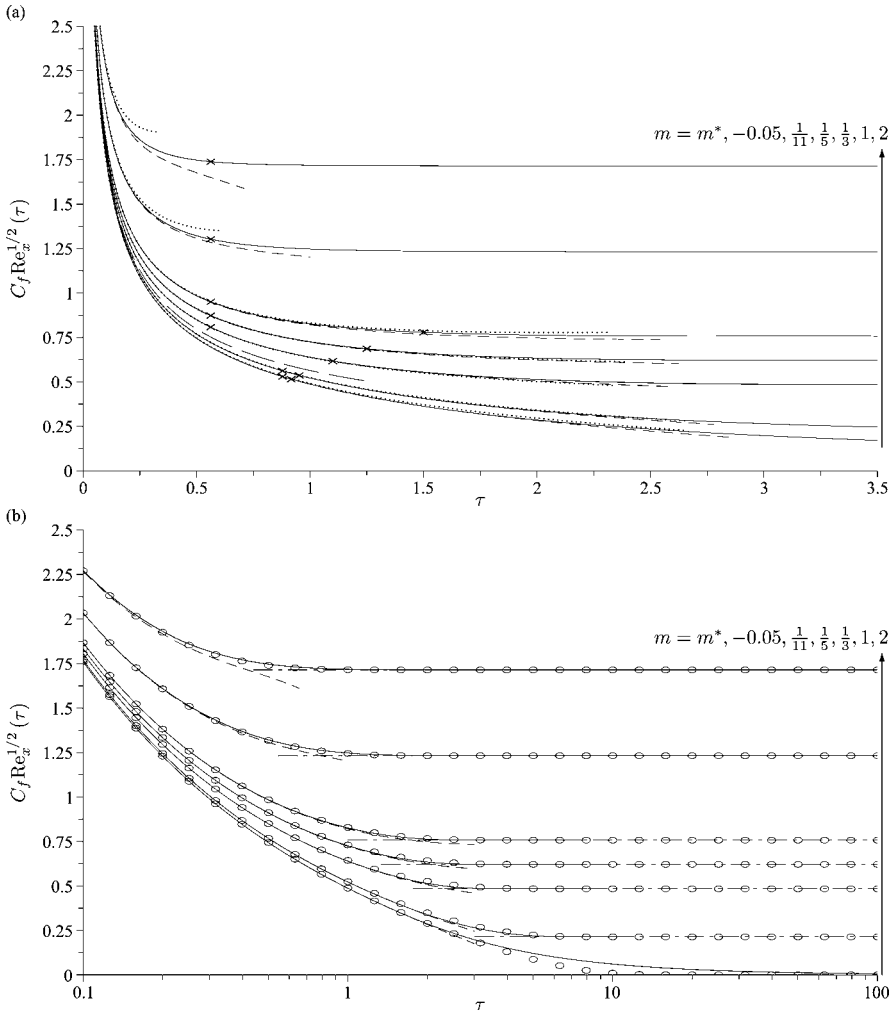

Notes: The symbols × in (a) indicate the times $\bar{\tau}$ and τ_n^* at which the transfers between the numerical solution techniques described in section 5 take place. The empirical approximation (47) is presented for each value of m using the symbols o; different values of m in comparison with (a) the small-time solution (21), using one (long-dashed line), two (dotted line), and three (dashed line) terms, (b) the three-term small-time solution (dashed line) together with the predicted large-time, steady-state value (dot-dash line), see Table III(a)

Figure 7.
Evolution of the non-dimensional skin friction coefficient $C_f(\tau)\mathrm{Re}_x^{1/2}$ for different values of m presented with a logarithmic horizontal τ axis

may be used with confidence over the whole time interval range of interest. The matching function for the non-dimensional skin friction coefficient has the following form (see Harris *et al.*, 2002):

$$C_f(\tau)\mathrm{Re}_x^{1/2} = \frac{1}{\sqrt{\pi}}\tau^{-1/2}\left[\pi(f''_\infty(0))^2\tau + \exp(-\alpha_1\tau - \gamma_1\tau^2)\right]^{1/2}, \qquad (47)$$

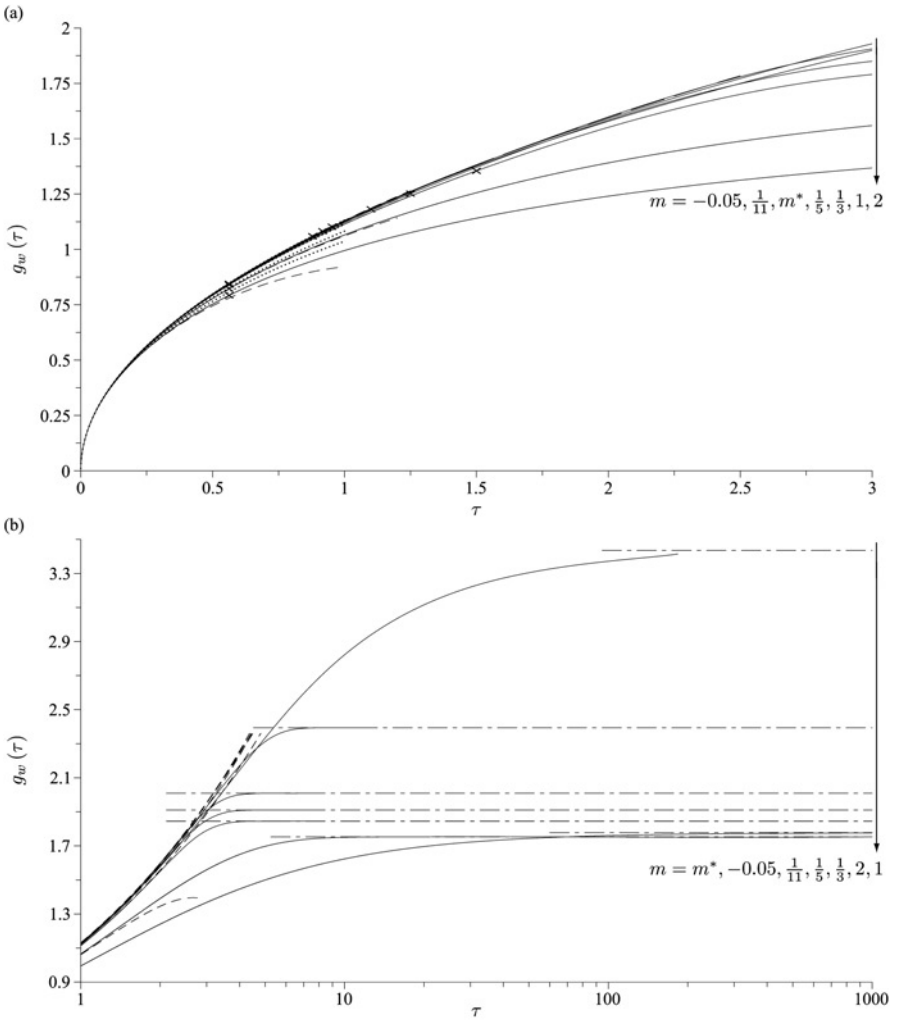

Figure 8.
Evolution of the reduced surface temperature $g_w(\tau)$ for different values of m when $\mathrm{Pr} = 1$ presented with a logarithmic horizontal τ axis

Notes: The symbols × in (a) indicate the times $\tilde{\tau}$ and τ_n^* at which the transfers between the numerical solution techniques described in Section 5 take place; different values of m when Pr = 1 in comparison with (a) the small-time solution (21), using one (long-dashed line), two (dotted line), and three (dashed line) terms, (b) the three-term small-time solution (dashed line) together with the predicted large-time, steady-state value (dot-dash line), see Table III(a)

where:

$$\alpha_1 = \pi(f''_\infty(0))^2 - 2m\left(1 + \frac{4}{3\pi}\right),$$

$$\gamma_1 = -\sqrt{\pi}F''_2(0) + \frac{1}{2}\pi^2(f''_\infty(0))^4 - 2m\pi\left(1 + \frac{4}{3\pi}\right)(f''_\infty(0))^2 + m^2\left(1 + \frac{4}{3\pi}\right)^2. \quad (48)$$

The comparison provided in Figure 7(b) between the empirical formula (47) and the full numerical solution for the non-dimensional skin friction coefficient $C_f(\tau)\mathrm{Re}_x^{1/2}$ demonstrates that this matching solution can be used with confidence over the whole range of values of τ for each of the values of m presented, and may therefore be used with confidence in engineering applications. A similar empirical formula was derived for the non-dimensional reduced surface temperature, but the transition from the small-time solution (21) to the steady-state solution was not as accurately modelled by this approximation, and therefore these results have not been presented.

6.2. Solutions for other values of Pr and m

As Pr and m were varied from $\mathrm{Pr} = 1$ and $m = 1/5$, the only parameters within the numerical procedures that required changing from the analysis in section 6.1, i.e. those parameters that produced any significant change in the solutions presented within the figures contained in this paper, were the values of η_∞ and τ_∞. The values stated below are sufficiently large for any further increase to produce results that are graphically indistinguishable from those presented in the figures. These increases in the values of η_∞ and τ_∞ reflect increases in the thermal and velocity boundary-layer thicknesses and the time required to reach a steady-state solution, as appropriate.

For $\mathrm{Pr} = 1$, further numerical solutions were determined for the cases of $m = m^*, -0.05, 1/11, 1/3, 1$, and 2, with necessary increases in η_∞ for $m = m^*$ and -0.05 to $\eta_\infty = 15$, resulting in a necessary increase in N to $N = 2000$, thereby maintaining the same value of the spatial grid increment for the step-by-step solution procedures. For $m \geq 1$, the forward-integrating approach does not break down, and therefore the matching numerical approach is not required. It should also be noted that the time at which the steady-state solution is reached has increased for $m = 2$ in comparison to $m = 1$.

The value of $\tau_\infty = 8$ was used for $m = 1/11$ and $1/3$, thereby requiring 1,825 and 1,720 temporal grid increments, respectively, according to the value of $\tau_n^* \approx 1/(1-m)$ and for the same time step discussed in section 6.1. However, the value of τ_∞ had to be increased for the chosen values of $m < 0$ and the matching numerical procedure required a significant increase in the computational time necessary to satisfy the convergence criterion. Accordingly, for $m = -0.05$, the value $\tau_\infty = 12$ and 2,923 temporal grid increments (again maintaining the time step used in section 6.1) were

	m						
	m^*	-0.05	1/11	1/5	1/3	1	2
(a)							
$f_\infty'(0)$	0.0	0.2134837	0.4837449	0.6213238	0.7574476	1.2325877	1.7150680
$g_\infty(0)$	3.4351892	2.3941161	2.0091890	1.9108082	1.8450971	1.7529551	1.7774736
(b)							
				Pr			
	0.72	1	2	5	10		
$g_\infty(0)$	2.1544588	1.9108082	1.4902233	1.0804608	0.8502618		

Notes: (a) different values of m when the Prandtl number $\mathrm{Pr} = 1$; (b) different values of the Prandtl number Pr when $m = 1/5$

Table III. The predicted steady-state values of the non-dimensional skin friction coefficient $C_f(\tau)\mathrm{Re}_x^{1/2} = f_\infty''(0)$ and the reduced surface temperature $g_w(\tau) = g_\infty(0)$, which are valid for large values of τ

used to produce the results presented in the figures. For $m = m^*$, the results presented here have been based upon $\tau_\infty = 200$ and 3,200 temporal grid increments (a time step of approximately 0.06221 that is significantly larger than that used in section 6.1); this calculation required a significant amount of computational time, namely of the order of 7,000 hours on a 2.66 GHz Intel Xeon processor. However, even for this intensive calculation for the case of $m = m^*$, this value of τ_∞ does not lead to a completely smooth approach to the predicted steady-state values of the appropriate quantities, and a value of τ_∞ beyond which a negligible effect on the numerical solution is observed may be beyond reasonable computational limitations if an accurate temporal grid increment is to be maintained.

As described in section 6.1 for $\mathrm{Pr} = 1$ and $m = 1/5$, the numerical and asymptotic solutions for the non-dimensional skin friction coefficient and the reduced surface temperature are presented in Figures 7 and 8, respectively, for the cases of $m = m^*$, -0.05, 1/11, 1/3, 1, and 2, when $\mathrm{Pr} = 1$. As for the case of $m = 1/5$, the range of validity of the one-term, small-time solution (21) is significantly improved when either two or three terms are used in this approximation. As m increases above $m = 1/5$, the range over which the corresponding small-time solutions are indistinguishable from the numerical solutions decreases. For $m^* \leq m \leq 1/5$, these three-term solutions are all valid until $\tau \approx$ 1-2, but this upper limit is significantly reduced to $\tau \approx 0.15$ for $m = 2$. As described above, for $m = m^*$, the value of τ_∞ could not be taken sufficiently large for the steady-state solutions for the non-dimensional skin friction coefficient and the reduced surface temperature to be approached smoothly. However, the large-time, steady-state values presented in Table III for $C_f(\tau)\mathrm{Re}_x^{1/2}$ and $g_w(\tau)$ are approached smoothly for the presented cases of $m \neq m^*$.

The evolutions of the non-dimensional fluid velocity and temperature profiles for the cases of $m = 1$, $m = 2$ and $m = m^*$, when $\mathrm{Pr} = 1$, are presented in Figures 5(b-d) and 6(b-d). The profiles for $m = 1$ and $m = 2$ are similar in nature to those for $m = 1/5$, being mostly plotted at the same time instants as those for $m = 1/5$. The clear differences are the expected reduction in the thermal and velocity boundary-layer thicknesses as m is increased from $m = 1/5$ to 2, and the significant increase in the time taken to reach the steady-state profile for the case of $m = 2$. The corresponding solution profiles for $m = m^*$ are significantly different in nature and reflect both an increase in the thermal and velocity boundary-layer thicknesses, and again a large increase in the time taken to reach the steady-state conditions.

In order to demonstrate the influence of the Prandtl number on the solution of this problem, the evolution of the reduced surface temperature $g_w(\tau)$ has been presented in Figure 9 for $\mathrm{Pr} = 0.72$, 1, 2, 5, and 10, when $m = 1/5$. Precisely the same numerical solution parameters as those described in section 6.1 for $\mathrm{Pr} = 1$ were used in each case, except that for $\mathrm{Pr} = 10$ it was necessary to change τ_∞ to $\tau_\infty = 12$, and correspondingly increase the number of temporal grid increments to 2,845 to maintain the same time step size. For each value of Pr, the reduced surface temperature is presented in comparison to the one-, two-, and three-term small-time solutions (21) and the large-time solution presented in Table III(b). In general, the inclusion of the second and third terms in the small-time solution (21) for the reduced surface temperature are each observed to extend the upper range of validity of this approximation. As Pr increases, so does the time τ taken to reach the steady-state solution for the reduced surface temperature, and the small-time approximations break down at an increasingly smaller proportion of the total transient time. The equivalent profiles to those shown in Figures 5 and 6 for $\mathrm{Pr} \neq 1$ are similar in nature and, therefore, have not been presented here.

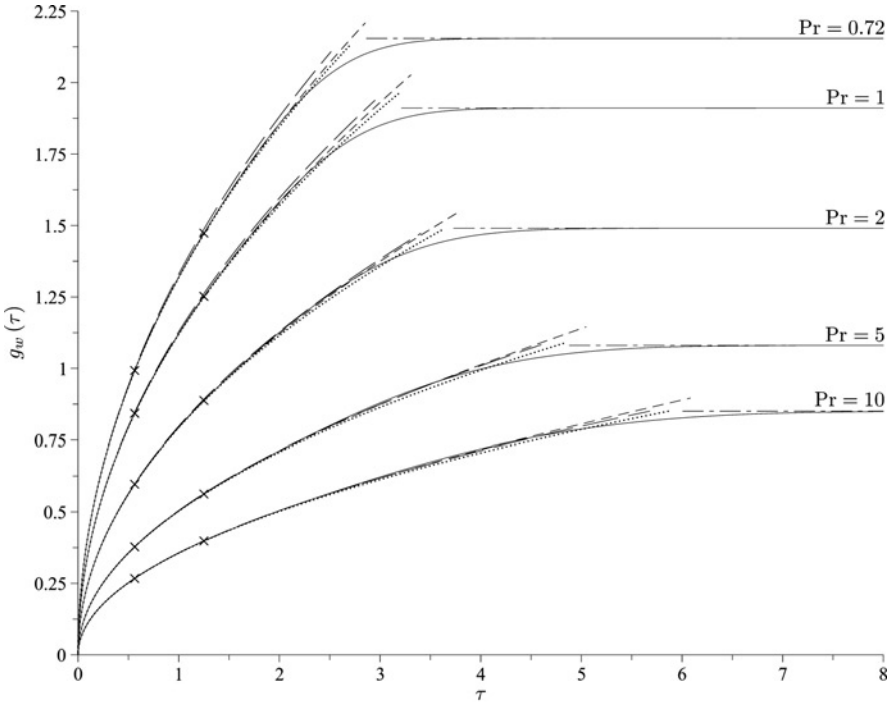

Notes: The symbols × indicate the times $\bar{\tau}$ and τ_n^* at which the transfers between the numerical solution techniques described in section 5 take place; surface temperature evolution is in comparison with the small-time solution (21), using one (long-dashed line), two (dotted line), and three (dashed line) terms, and the predicted large-time, steady-state value (dot-dash line), see Table III(b)

Figure 9.
Evolution of the reduced surface temperature $g_w(\tau)$ for different values of the Prandtl number Pr when $m = 1/5$

7. Conclusions

Detailed solutions for both the momentum (Falkner-Skan) and heat transfer (energy) equations in the unsteady, laminar boundary-layer flows past a semi-infinite wedge have been presented, where the unsteadiness was caused by the impulsive motion of the free stream velocity and by the sudden change in the surface heat flux. Small-time (initial unsteady flow) and large-time (steady-state flow) analytical solutions have been presented, but, since these approximations rapidly build up in complexity, the majority of the solutions have been obtained numerically. The partial differential equations governing the flow and heat transfer have been solved numerically using an implicit finite-difference scheme as proposed by Merkin (1972), and for the situations in which this forward-integration approach breaks down at later times the numerical solution has been completed using the matching technique of Dennis (1972). The analytical time series solutions that are valid for small times may be used to check the results derived in the early stages of the time-dependent integration, and/or even to commence the integration. Further, this investigation has also focussed on investigating the fluid flow and heat transfer developments at large times, namely when the skin friction coefficient and the surface temperature have closely approached the values that they would assume at an infinite time (steady-state flow and heat transfer).

References

Bhattacharyya, S. and Gupta, A.S. (1996), "Transient compressible boundary layer on a wedge impulsively set into motion", *Archive of Applied Mechanics*, Vol. 66, pp. 336-42.

Cheng, W.T. and Lin, H.T. (2002), "Non-similarity solution and correlation of transient heat transfer in laminar boundary layer flow over a wedge", *International Journal of Engineering Science*, Vol. 40, pp. 531-48.

Dennis, S.C.R. (1972), "The motion of a viscous fluid past an impulsively started semi-infinite flat plate", *Journal of the Institute of Mathematics of its Applications*, Vol. 10, pp. 105-17.

Hall, M.G. (1969), "The boundary layer over an impulsively started flat plate", *Proceedings of the Royal Society of London A*, Vol. 310, pp. 401-14.

Harris, S.D., Ingham, D.B. and Pop, I. (1997a), "Free convection from a vertical plate in a porous media subjected to a sudden change in surface temperature", *Intermational Communications in Heat Mass Transfer*, Vol. 24, pp. 543-52.

Harris, S.D., Ingham, D.B. and Pop, I. (1997b), "Free convection from a vertical plate in a porous medium subjected to a sudden change in surface heat flux", *Transport in Porous Media*, Vol. 26, pp. 207-26.

Harris, S.D., Ingham, D.B. and Pop, I. (1999), "Unsteady mixed convection boundary-layer flow on a vertical surface in a porous medium", *International Journal of Heat and Mass Transfer*, Vol. 42, pp. 357-72.

Harris, S.D., Ingham, D.B., and Pop, I. (2001), "Transient boundary-layer heat transfer from a flat plate subjected to a sudden change in heat flux", *European Journal of Mechanics B-Fluids*, Vol. 20, pp. 187-204.

Harris, S.D., Ingham, D.B. and Pop, I. (2002), "Unsteady heat transfer in impulsive Falkner-Skan flows: constant wall temperature case", *European Journal of B-Fluids*, Vol. 21, pp. 447-68.

Harris, S.D., Ingham, D.B. and Pop, I. (2008), "Unsteady heat transfer in impulsive Falkner-Skan flows: constant wall heat flux case", *Acta Mechanica*. Vol. 20, pp. 185-96.

Harris, S.D., Elliott, L., Ingham, D.B. and Pop, I. (1998), "Transient free convection flow past a vertical flat plate subjected to a sudden change in surface temperature", *International Journal of Heat and Mass Transfer*, Vol. 41, pp. 357-72.

Hartree, D.R. (1937), "On an equation occurring in Falkner and Skan's approximate treatment of the equations of the boundary layer", *Proceedings of the Cambridge Philosophical Society*, Vol. 33, pp. 223-39.

Kuo, B.-L. (2003), "Application of the differential transformation method to the solutions of Falkner-Skan wedge flow", *Acta Mechanica*, Vol. 164, pp. 161-74.

Lin, H.-T. and Lin, L.-K. (1987), "Similarity solutions for laminar forced convection heat transfer from wedges to fluids of any Prandtl number", *International Journal of Heat Mass Transfer*, Vol. 30, pp. 1111-18.

Ludlow, D.K., Clarkson, P.A. and Bassom, A.P. (2000), "New similarity solutions of the unsteady incompressible boundary-layer equations", *Quarterly Journal of Mechanics and Applied Mathematics*, Vol. 53, pp. 175-206.

Merkin, J.H. (1972), "Free convection with blowing and suction", *International Journal of Heat Mass Transfer*, Vol. 15, pp. 989-99.

Nanbu, K. (1971), "Unsteady Falkner-Skan flow", *Journal of Applied Mathematics and Physics (ZAMP)*, Vol. 22, pp. 1167-1172.

Pantokratoras, A. (2006), "The Falkner-Skan flow with constant wall temperature and variable viscosity", *International Journal of Thermal Science*, Vol. 45, pp. 378-89.

Pop, I. (1996), "Transient heat transfer in boundary-layer flows", *Proceedings of the International Symposium on Transient Convective Heat Transfer, Cesme, 19-23 August,* Padet, J. and Arinç, F. (Eds), Begell House, New York, NY, pp. 3-17.

Riley, N. (1975), "Unsteady laminar boundary layers", *SIAM Review*, Vol. 17, pp. 274-97.

Riley, N. (1990), "Unsteady viscous flows", *Science Progress Oxford*, Vol. 74, pp. 361-77.

Smith, S.H. (1967), "The impulsive motion of a wedge in a viscous fluid", *Journal of Applied Mathematics and Physics (ZAMP)*, Vol. 18, pp. 508-22.

Stewartson, K. (1951), "On the impulsive motion of a flat plate in a viscous fluid", *Quarterly Journal of Mechanics and Applied Mathematics*, Vol. 4, pp. 182-98.

Telionis, D.R. (1979), "Review–unsteady boundary layers, separated and attached", *Journal of Fluids Engineering*, Vol. 101, pp. 29-43.

Telionis, D.R. (1981), *Unsteady Viscous Flows*, Springer, New York, NY.

Tsay, S.-Y. and Shih, Y.-P. (1979), "Laminar forced convection in wedge flow with separation", *Journal of Chinese Institute of Engineers*, Vol. 2, pp. 53-7.

Watkins, Jr, C.B. (1976), "Unsteady heat transfer in impulsive Falkner-Skan flows", *International Journal of Heat and Mass Transfer*, Vol. 19, pp. 395-403.

Williams, J.C. and Rhyne, T.B. (1980), "Boundary-layer development on a wedge impulsively set into motion", *SIAM Journal of Applied Mathematics*, Vol. 38, pp. 215-24.

Xu, H. and Pop, I. (2008), "Unsteady boundary-layer flow started impulsively from rest along a symmetric wedge", *Journal of Applied Mathematics and Mechanics (ZAMM)*, Vol. 88, pp. 507-14.

About the authors

Simon D. Harris' fields of interest include applied mathematics: fluid mechanics, heat transfer, CFD, multiphase fluid flow through faults, boundary-layer theory, convective flow in fluid-saturated porous media, genetic algorithms, inverse problems.

Derek B. Ingham's fields of interest include applied mathematics: fluid mechanics, heat transfer, CFD, particle dynamics, aerosols, fuel cells, boundary-layer theory, convective flow in fluid-saturated porous media, genetic algorithms, ventilation, boundary integral methods, inverse problems.

Ioan Pop's fields of interest include applied mathematics: fluid mechanics and heat transfer with application to boundary-layer theory, heat transfer in Newtonian and non-Newtonian fluids, convective flow in fluid-saturated porous media, magnetohydrodynamics. Ioan Pop is the corresponding author and can be contacted at pop.ioan@yahoo.co.uk